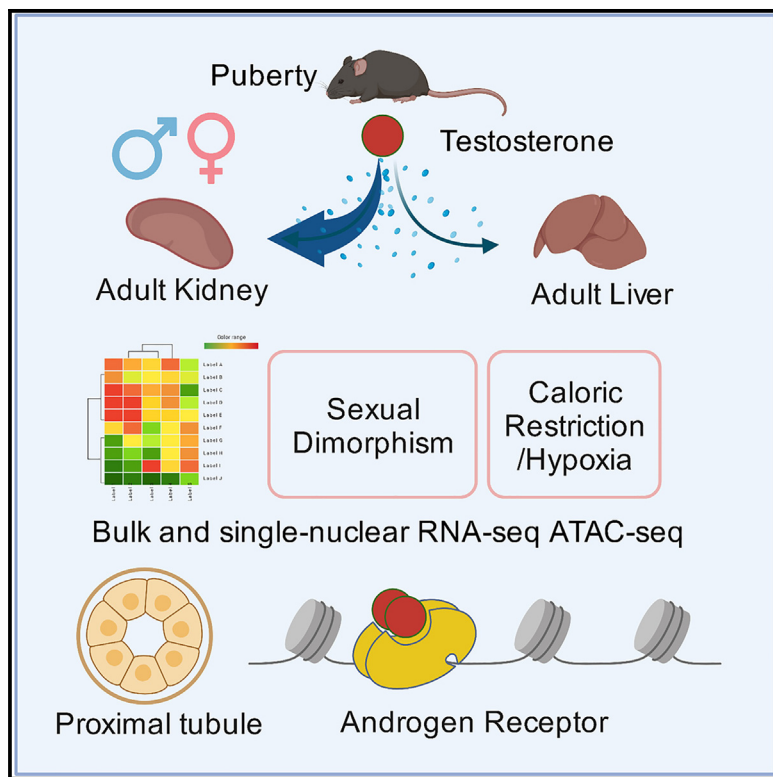


Direct androgen receptor control of sexually dimorphic gene expression in the mammalian kidney

Graphical abstract



Authors

Lingyun Xiong, Jing Liu,
Seung Yub Han, ..., Junhyong Kim,
Adam L. MacLean,
Andrew P. McMahon

Correspondence

amcmahon@med.usc.edu

In brief

Xiong and Liu et al. show that in the mouse kidney, androgen receptor-mediated transcription establishes distinct molecular and physiological states between sexes and proximal tubule segments. Disease-modifying regimens correlate with altered kidney sex profiles, and mouse/human kidneys show limited conservation in sexually dimorphic gene control.

Highlights

- Sex differences in kidney proximal tubule cells are determined by testicular androgens
- Single-nuclear multiomics identify direct targets of androgen receptors in kidneys
- Contrasting control of sexual dimorphism between organs and mouse and human kidneys
- Disease-modifying regimens correlate with altered sex profiles in the kidney

Article

Direct androgen receptor control of sexually dimorphic gene expression in the mammalian kidney

Lingyun Xiong,^{1,2,8,10} Jing Liu,^{1,8} Seung Yub Han,³ Kari Koppitch,¹ Jin-Jin Guo,¹ Megan Rommelfanger,² Zhen Miao,³ Fan Gao,^{4,9} Ingileif B. Hallgrimsdottir,⁵ Lior Pachter,^{5,6} Junhyong Kim,⁷ Adam L. MacLean,² and Andrew P. McMahon^{1,11,*}

¹Department of Stem Cell Biology and Regenerative Medicine, Eli and Edythe Broad Center for Regenerative Medicine and Stem Cell Research, Keck School of Medicine of the University of Southern California, Los Angeles, CA 90089, USA

²Department of Quantitative and Computational Biology, University of Southern California, Los Angeles, CA 90089, USA

³Graduate Program in Genomics and Computational Biology, Biomedical Graduate Studies, University of Pennsylvania, Philadelphia, PA 19104, USA

⁴Caltech Bioinformatics Resource Center at Beckman Institute, California Institute of Technology, Pasadena, CA 91125, USA

⁵Division of Biology and Biological Engineering, California Institute of Technology, Pasadena, CA 91125, USA

⁶Department of Computing and Mathematical Sciences, California Institute of Technology, Pasadena, CA 91125, USA

⁷Department of Biology, University of Pennsylvania, Philadelphia, PA 19104, USA

⁸Present Address: Department of Integrative Biology and Physiology, University of California, Los Angeles, CA 90095 USA

⁹Present Address: Lyterian Therapeutics, San Francisco, California, USA

¹⁰These authors contributed equally

¹¹Lead contact

*Correspondence: amcmahon@med.usc.edu

<https://doi.org/10.1016/j.devcel.2023.08.010>

SUMMARY

Mammalian organs exhibit distinct physiology, disease susceptibility, and injury responses between the sexes. In the mouse kidney, sexually dimorphic gene activity maps predominantly to proximal tubule (PT) segments. Bulk RNA sequencing (RNA-seq) data demonstrated that sex differences were established from 4 and 8 weeks after birth under gonadal control. Hormone injection studies and genetic removal of androgen and estrogen receptors demonstrated androgen receptor (AR)-mediated regulation of gene activity in PT cells as the regulatory mechanism. Interestingly, caloric restriction feminizes the male kidney. Single-nuclear multiomic analysis identified putative *cis*-regulatory regions and cooperating factors mediating PT responses to AR activity in the mouse kidney. In the human kidney, a limited set of genes showed conserved sex-linked regulation, whereas analysis of the mouse liver underscored organ-specific differences in the regulation of sexually dimorphic gene expression. These findings raise interesting questions on the evolution, physiological significance, disease, and metabolic linkage of sexually dimorphic gene activity.

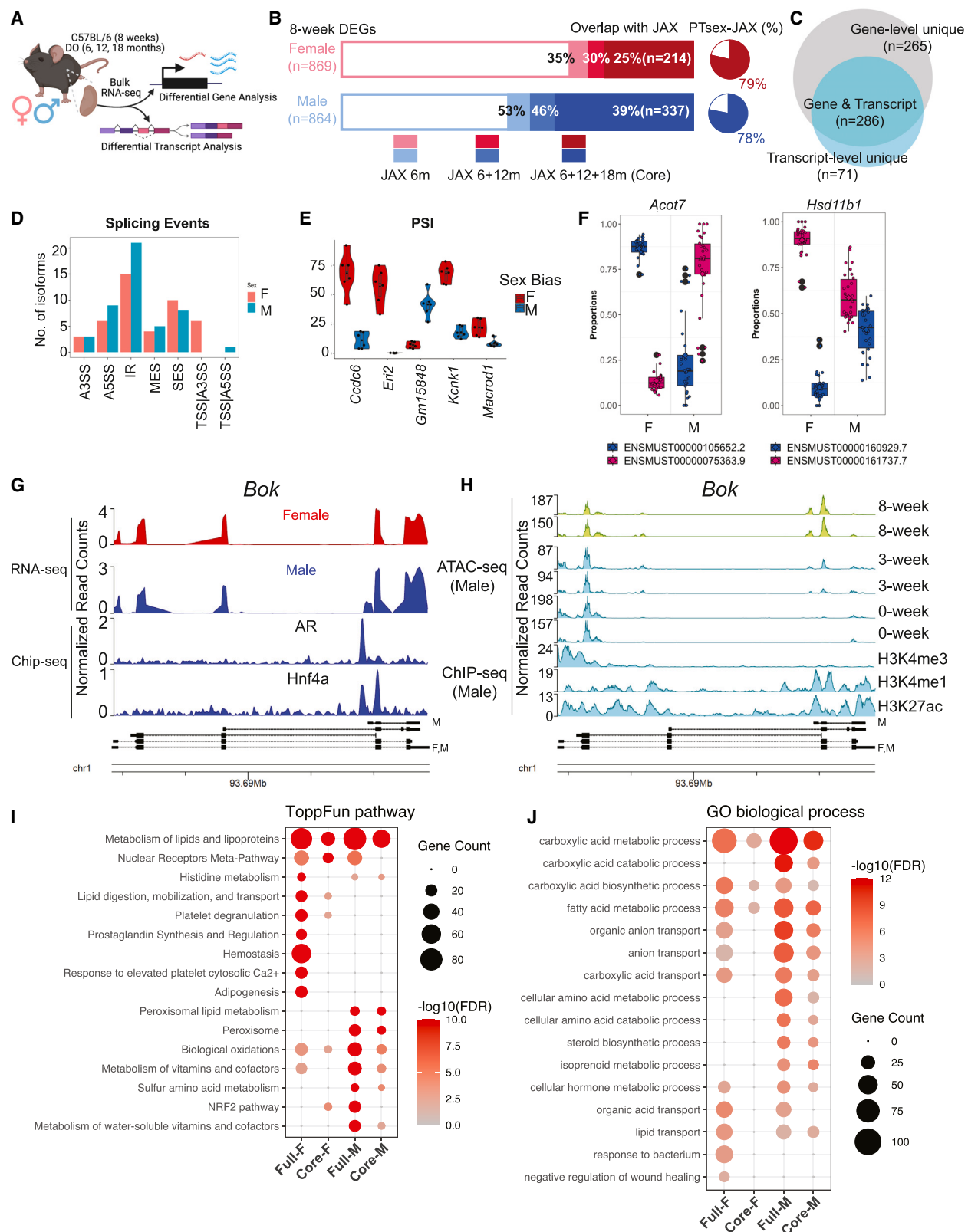
INTRODUCTION

Increasing evidence points to differences in epidemiology, pathophysiology, drug responsiveness, and disease outcomes between the sexes. For example, human kidney studies indicate age-related decline in renal function is faster in men than in age-matched premenopausal women.¹ Further, chronic disease tends to be more aggressive in men and progresses to end-stage renal disease more rapidly than in women.^{1,2} Men are more susceptible to acute kidney injury, while women are resilient and show improved tolerance to renal ischemia.^{3–5} Sex-dependent response to kidney diseases has also been reported in rodents.^{5–7} An improved understanding of cellular roles and molecular controls in the male and female kidney will advance our understanding of renal function and renal disease mechanisms between the sexes.

In the mouse, the most widely studied mammalian model, researchers have identified differences in cellular morphology,^{8–11} renal physiology,^{12–14} and cell-type-specific gene expression^{15–18}

over the last three decades. More recently, a detailed single-cell analysis of gene expression throughout the adult mouse kidney identified 984 genes with sex-biased expression, highlighting proximal tubule (PT) segments as the predominant cellular source of sex-specific variability in gene expression,¹⁹ and microdissection and multiomics approaches identified sex differences in transcription, chromatin accessibility, and proteinomics.²⁰ PT cell types play a central role in renal physiology responsible for the primary resorption and recovery of essential molecules from the initial renal filtrate, including glucose, salts, and water, as well as a variety of other important cellular functions such as gluconeogenesis and molecular detoxification.^{21,22}

Sex hormones have long been associated with sex differences in the structure and function of the kidney.^{23–25} Androgens enhance salt reabsorption²⁶ and water handling²⁷ in the PT and stimulate total kidney volume in males.^{26,28} Testosterone has also been shown to modulate urinary calcium clearance,²⁹ as well as ammonia metabolism and excretion.^{30,31} Gonadal removal and hormone injection studies point to a



(legend on next page)

role for testosterone regulation of sexual dimorphism in both the mouse and rat kidney.^{23,30–38} However, the direct actions of sex hormones and their receptors in regulating sex-biased transcription in the PT have not been studied. Regulatory control of sex-dependent gene expression in the liver has revealed that sex hormones act at the level of the hypothalamic-pituitary axis to control the release of growth hormone (GH), the direct regulator of sexual dimorphic gene expression in hepatocytes.^{39–44}

In this study, we investigated the temporal, spatial, and genomic regulation of sex hormone action in the mouse kidney. In contrast to the liver, testosterone is the primary and direct driver of sexual dimorphism, acting through androgen receptor (AR) regulation of chromatin accessibility in PT cell types. Complementary genetic studies in the liver revealed a hitherto unrecognized component of direct Ar action on hepatocyte gene expression, with a conserved sex bias in expression of shared genes with the mouse kidney. Comparing gene expression in the mouse and human kidney identified few non-sex-chromosome-linked sex-biased genes between the sexes, but a conserved sex bias was observed in their expression.

RESULTS

Gene- and transcript-level renal sex differences in adult mice

To identify a set of sex-biased genes that are invariant with respect to age, mouse strain, and technology assessing gene activity (Figure 1A), we first examined differential gene expression between male and female kidneys in 8-week C57BL/6 mice using whole-kidney bulk RNA sequencing (RNA-seq), identifying 1,733 genes with sex-biased expression: 869 expressed at higher levels in the female kidney (female [F]-biased) and 864 expressed at higher levels in the male kidney (male [M]-biased; Table S1.1; the full set). We compared this gene set with renal sex differences identified among genetically diverse mice at 6, 12, and 18 months⁴⁵ (GSE121330, referred to as the JAX data hereafter) identifying 214 F-biased genes (25%) and 337 M-biased genes (39%) with consistent sex bias across all whole-kidney bulk RNA-seq datasets (551 genes in total; Figure 1B; Table S1.2). This core set of sex-biased genes overlapped significantly with sex-biased gene expression identified in PT segments from single-cell RNA-seq (scRNA-seq) analysis¹⁹ (PT-sex genes; hypergeometric test, $p = 6.0E-27$ in female, $p = 6.5E-39$ in male; Figure S1A). Moreover, the core set in-

cludes 78%–79% of the PT-sex genes that exhibited persistent sex bias from 6 to 18 months (Figure 1B), including several transcriptional regulators such as *Foxq1* (F-biased) and *Nr1h4* (M-biased).

At the transcript level, we defined a core set of sex-biased isoforms using the same criteria (Figure S1B). Among the 551 sex-biased genes in the core set, 286 (52%) also showed sex bias in transcript usage (Figure 1C). Interestingly, 71 genes that did not exhibit sex difference at the level of overall gene expression were found to show sex difference at the transcript level (Figure 1C; Table S1.3). Transcript-level sex differences manifest in a variety of alternative splicing events (Figure 1D), including alternative 5' splice site usage (*Ccdc6*, *Kcnk1*, and *Macrod1*) and intron retention (*Eri2* and *Gm15848*) (Figure 1E; Figure S1C). Among the 286 genes exhibiting sex differences at gene and transcript level, *Acot7* (F-biased) and *Hsd11b1* (M-biased) showed the largest disparity in transcript usage (Figure 1F; Figure S1D). In addition, adult male kidneys express a short isoform of *Bok* (encoding BCL2 Family Apoptosis Regulator) through alternative promoter usage. Comparison of *Bok* transcripts with published studies of Ar chromatin association in the male kidney⁴⁶ and epigenomic histone modifications (H3K4me1 and H3K27ac⁴⁸) in adult male kidneys (Figures 1G–1H) indicate the male-specific short isoform of *Bok* has proximal AR binding associated with chromatin opening in the maturing postnatal kidney⁴⁷ (Figure 1H).

Functional enrichment analysis based on our sex-biased genes and isoforms provided insights into the dimorphic functionalities in the kidney. Using ToppCluster,⁴⁹ both sexes showed a significant enrichment in pathways associated with metabolism and lipid lipoproteins, males showed a strong bias in peroxisome lipid metabolism (Figure 1I; Figure S1E). The male kidney exhibits enhanced expression of the fatty acid translocase *Cd36*⁵⁰ and acyl-coenzyme A oxidase 1 (encoded by *Acox1*) which catalyzes the first step in peroxisomal fatty acid degradation⁵¹ while the female kidney shows elevated expression of genes involved in lipid synthesis (*Scd1*),⁵² lipid digestion and mobilization (*Fabp1*),⁵³ and the prevention of lipotoxicity (*Acot7*).⁵⁴ Nuclear receptors (NRs), which play important roles in maintaining renal function,⁵⁵ show differential enrichment in sex-biased gene expression. *Nr1h4*, encoding the farnesoid X receptor (FXR), is associated with the metabolic shift from synthesis to the oxidation and catabolism of lipids and exhibits a M-bias.

By contrast, expression of several NRs associated with xenobiotic metabolism showed an F-bias: *Nr1h3*, encoding liver X receptor (LXR); *Nr1i2*, encoding pregnane X receptor (PXR); *Nr1i3*,

Figure 1. Gene- and transcript-level renal sex differences in adult mice

(A) Schematic summary of the computational analyses of renal transcriptome in adult male and female mice. Created with BioRender.com.

(B) Stacked bar plot showing the proportion of sex-biased genes in 8-week C57BL/6 mice with continuing sex bias in the aged kidney of diversity outbred (DO) mice (the JAX data⁴⁵). Pie charts represent the percentage of core sex-biased genes that were identified in the PT segments from previous single-cell RNA-seq (scRNA-seq) experiment.¹⁹

(C) Venn diagram compares renal sex differences revealed by gene- and transcript-level analysis.

(D) Bar plot shows the distribution of dimorphic isoforms with alternative splicing events in the male and female kidneys.

(E) Distribution of percent spliced-in values for top genes showing dimorphic splicing events in the male and female kidneys.

(F) Dimorphic transcript usage of distinct isoform in *Acot7* (F-biased) and *Hsd11b1* (M-biased) in male and female kidneys.

(G and H) Coverage plot over the genomic region of *Bok* by bulk RNA-seq in male and female kidneys, aligned with data from ChIP-seq experiment against AR and *Hnf4a* in the male kidneys⁴⁶ (G) and by ATAC-seq experiment in the male kidneys,⁴⁷ aligned with ENCODE data from ChIP-seq experiment against epigenetic biomarkers⁴⁸ (H).

(I and J) Dot plot shows the enrichment of ToppFun pathways (I) and gene ontology terms (J) for both the full and core set of sex-biased genes.

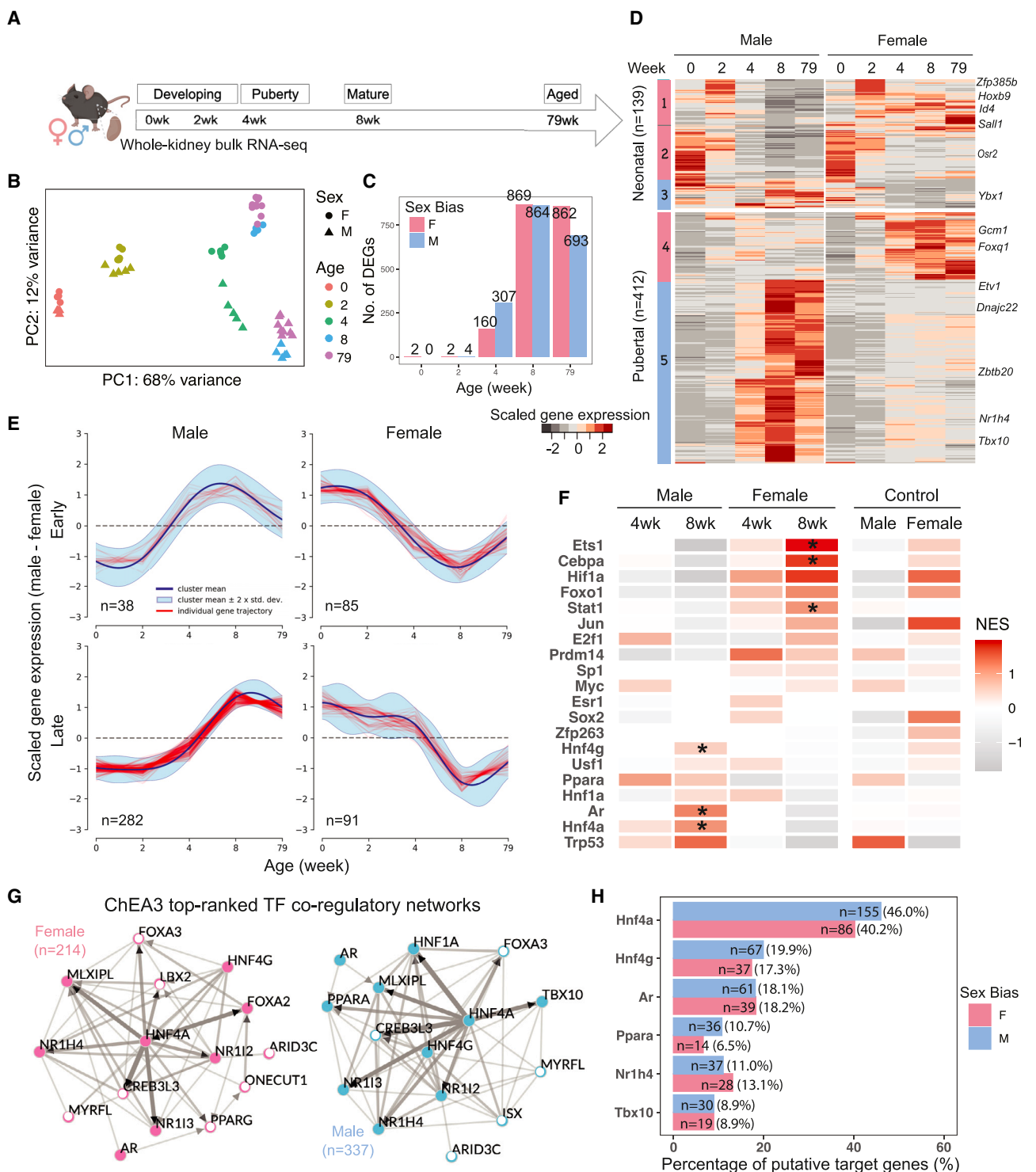


Figure 2. Male and female renal transcriptomes diverge at puberty

(A) Schematic summary of the experimental design in sampling renal transcriptome in male and female C57BL/6 mice. Created with BioRender.com.

(B) Principal-component analysis (PCA) reveals that the distribution of sample variations in gene expression is most influenced by age and sex.

(C) Bar plot demonstrates the number of sex-biased genes identified at individual time points via differential expression analysis.

(D) Heatmap shows the scaled average expression levels of the core sex-biased genes in male and female samples at individual time points.

(E) Representative clusters of divergent gene expression dynamics analyzed by DPGP.⁵⁷ Red tracings represent genes, the navy line represents the mean divergent gene expression of the cluster, and the cyan margin shows the 95% confidence interval.

(legend continued on next page)

encoding constitutive androstane receptor (CAR); and *Rxrg*, encoding the retinoid X receptor gamma sub-unit (RXR γ). In addition, gene ontology (GO) terms for carboxylic acid degradation, amino acid metabolism, and steroid biosynthesis were more strongly associated with male kidneys, while female kidneys showed GO term bias associated with bacteria response and negative regulation of wound healing (Figure 1J).

Male and female renal transcriptomes diverge at puberty between 3 and 8 weeks

To understand how dimorphic gene expression arises in the mouse kidney,⁵⁶ we performed bulk RNA-seq analysis of C57BL/6 male and female kidneys at 0, 2, 4, 8, and 79 weeks postpartum and identified differences in mRNA transcripts between the sexes (Figure 2A). Principal-component analysis (PCA) highlighted age (PC1) and sex (PC2) as the leading components of variation in gene expression among the kidney samples, and sex differences became evident from 4 weeks (Figure 2B). Differential gene expression between male and female kidneys was assessed at each time point (Figure 2C; Table S1). In the newborn and 2-week kidney, only sex-chromosome encoded genes distinguished the two sexes: 0- and 2-week F-bias in expression of X-linked *Xist* gene and 2-week M-bias in expression of Y-linked genes *Ddx3y*, *Eif2s3y*, *Uty*, and *Kdm5d* (Tables S1.4 and S1.5). By contrast, a pronounced sex bias was observed in a large number of autosomal genes at 4 weeks as mice entered puberty (457 of the 467 genes [97.6%] displaying sex bias; Table S1.6), which was further enhanced in the kidney at sexual maturity (8 weeks; 1,680 of 1,733 genes [96.9%] displaying sex bias Table S1.1) and late life (79 weeks; 1,504 of genes [96.7%] displaying sex bias; Table S1.7).

Comparing individual gene expression levels among the core gene set across all five time points revealed two broad categories of expression patterns (Figure 2D): developmental genes highly expressed at the earlier time points independent of sex (139 neonatal genes; 25%) and genes activated during puberty (4–8 weeks) many of which encode proteins participating in renal PT physiology (Table S1.2; 412 pubertal genes; 75%). Ninety percent of genes with M-biased expression (302 of the 337 M-biased genes) showed elevated expression between 4 to 8 weeks, including the transcriptional regulator encoding genes *Nr1h4* and *Tbx10* (Figure 2D; Figure S2G). By contrast, 51% of F-biased genes showed a similar trend in gene expression (Figure S2C). In summary, for the male kidney, expression of most M-biased genes was induced, while about half of the F-biased genes were suppressed during puberty.

Examining expression dynamics of the core sex-biased genes over time using a Dirichlet process Gaussian process mixture (DPGP) model,⁵⁷ we identified two major patterns (Figure 2E; Table S1.2): genes whose expression diverged early, before 4 weeks, and those diverging later, on or after 4 weeks (late).

The anti-correlation of dynamic features among M-early and F-early genes (Figure 2E) is suggestive of concomitant regulation during puberty whereby factors activate the male program and suppress the female program.

To predict the upstream regulators for the divergence of male and female renal transcriptomes, we performed transcription factor (TF) regulon analysis on high-confidence curated TFs using DoRothEA.^{58,59} Several TFs were predicted to specifically regulate the sex-biased program (Figure 2F): AR (Ar) and hepatocyte nuclear factor 1 alpha (Hnf1a), 4 alpha (Hnf4a), and gamma (Hnf4g) for M-biased program; CCAAT/enhancer-binding protein alpha (Cebpa), hypoxia-induced factor 1 alpha (Hif1a), and JAK-STAT pathway for F-biased program. We noted slight enrichment for ER α (Esr1) activity at 4 weeks for activating female program but not at 8 weeks (Figure 2F).

To explore the role of less-known TFs, we ranked factors that potentially regulate the expression of the core sex-biased genes using ChEA3.⁶⁰ As expected, Hnf4a, as an important proximal tubular cell fate regulator during kidney development,⁶¹ was centered as a hub that potentially regulated over 40% of both programs (Figures 2G and 2H). We found that Hnf4a not only binds to and activates the expression of *Ar*, *Tbx10*, and *Nr1h4* (chromatin immunoprecipitation sequencing [ChIP-seq] evidence⁶¹) but can also mediate the expression of M-biased genes (e.g., *Dnajc22*, *Ybx1*, and *Zbtb20*) and F-biased genes (e.g., *Gcm1* and *Foxq1*) (*in silico* prediction⁶⁰). AR could also regulate the expression of both programs (Figure 2H), where there are substantial overlaps between putative targets of Hnf4a and AR (75 of 100, 75%; e.g., *Ppara*), consistent with previous findings.⁴⁶ In summary, these computational predictions suggest Hnf4a acts as a key upstream regulator for both male and female sex programs in PT cells, whereas AR plausibly regulates sex differences in the male kidney.

The role of gonads, sex hormones, and sex hormone receptors in renal sex differences

Considering the emergence of renal sex differences at puberty and predicted involvement of AR regulation, we carried out a series of perturbation experiments to evaluate the role of AR, assaying responses through whole-kidney bulk RNA-seq (Figure 3A). First, to understand the influence of the endogenous sex hormones, we performed prepubertal gonadectomy in mouse models (castration in males [CM] and ovariectomy in females [OF]) at 3 weeks and assayed kidney gene expression between the sexes at 8 weeks. Second, to investigate the effect of exogenous androgen, we injected testosterone subcutaneously into castrated males and ovariectomized females at 8 weeks, examining the kidney response 24 h post-injection. Third, to study the role of sex hormone receptors directly on PT cells, we generated nephron-specific removal of Ar (Six2-Ar-knockout [KO]) and Esr1 (Six2-Esr1-KO), then assayed kidneys at 8 weeks.

(F) Tile map shows the predicted TF activities based on normalized gene expression in samples by DoRothEA,^{58,59} where high-confidence predictions are indicated by asterisks.

(G) Network diagram of top 15 TFs that were predicted by ChEA3⁶⁰ to regulate the core female and male programs. Edges indicate physical interaction supported by literature evidence, directed if supported by ChIP-seq data. Solid nodes indicate TFs that are expressed in the PT segments in our previous scRNA-seq experiment¹⁹; open circles represent those that are not expressed.

(H) Bar plot shows the percentage of putative targets among the core sex-biased genes that could be regulated by representative TFs, as predicted by ChEA3.⁶⁰ The number of putative targets is listed.

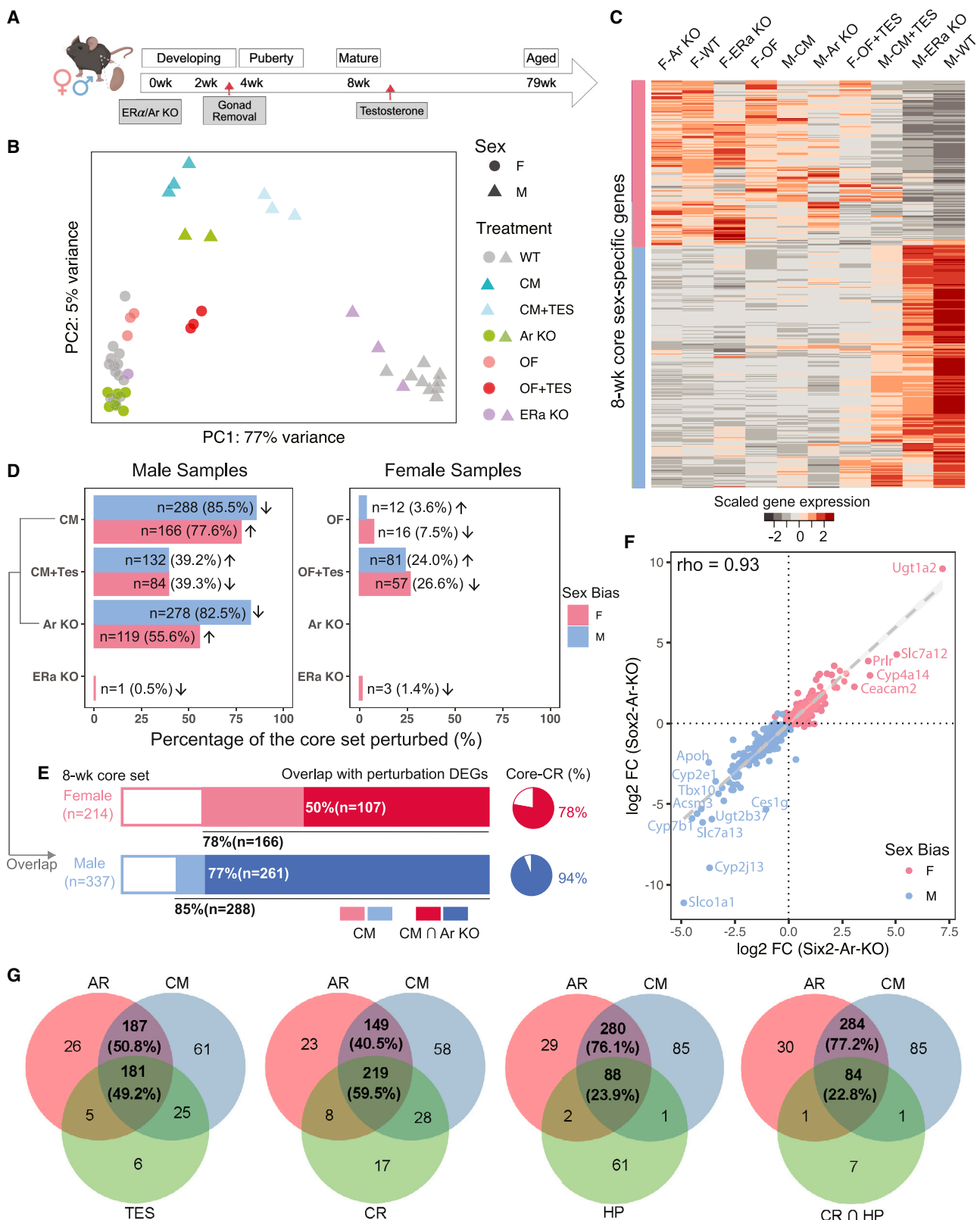


Figure 3. The role of gonads, sex hormones, and sex hormone receptors in renal sex differences

(A) The schematic summarizes the experimental design of perturbation treatments. Whole-kidney bulk RNA-seq was performed between 8–12 weeks. Created with BioRender.com.

(legend continued on next page)

Six2-CRE activity in nephron progenitor cells removes any potential sex hormone input from nephron progenitors and their nephron derivatives from the onset of embryonic kidney development.⁶³

A comparative analysis of all the above against relevant control samples via PCA showed that castration and nephron-specific AR removal had similarly strong effects: partially feminizing the male kidney (Figures 3B and 3C). After castration, 85.5% of the core M-biased genes (288 of 337) were down-regulated, and 77.6% of core F-biased genes (166 of 214) were up-regulated (Figure 3D; Figure S3A). On nephron-specific AR removal, a comparable number of sex-biased genes showed a significant change in expression: 82.5% of core M-biased genes (278 of 337) were down-regulated, whereas 55.6% of core F-biased genes (119 of 214) were up-regulated. Most (93.9%; 261 of 278) of the AR-dependent M-biased core gene set were also down-regulated in the castration experiment (Figure 3E). Transient administration of testosterone partially restored the male phenotype following castration and activated a male-like program in ovariectomized females (Figures 3B–3D; Tables S2.1–S2.4). By contrast, nephron removal of either *Ar* or *Esr1* had little effect on gene expression in the female kidney, in line with ovary removal and computational predictions (Figures 2F and 3B–3D; Tables S2.5–S2.8).

Comparing male kidneys following systemic whole-body AR removal through CRE-mediated recombination at embryonic implantation (*Sox2-Ar-KO*; Table S2.9) with nephron-specific removal (*Six2-Ar-KO*) showed a high concordance in the male kidney gene expression datasets (Spearman correlation rho = 0.93; Figure 3F), comparable to male-female comparisons (Figures S3B and S3C). A list of AR-responsive genes is presented in Table S2.10. In summary, systemic removal of *Ar* was equivalent to local removal of *Ar* in the nephron consistent with direct action of AR in PT cells.

Preconditioning by caloric restriction (CR) has been shown to mitigate risk to ischemia-reperfusion injury (IRI) in the mouse kidney.⁶² By comparing against the published kidney RNA-seq dataset on CR, we found that 59.5% of the 368 core set of genes responsive to both AR removal and castration were altered in male mice after a regimen of 4-week reduced food intake (Figure 3G). Note that 78% of CR-up-regulated genes are AR-responsive (F-biased) and 94% of CR-down-regulated genes are AR-responsive (M-biased) (Figure 3E). Moreover, for AR-responsive genes with large effect sizes ($\log_2 FC > 4$), the sets perturbed by CR and testosterone treatments were identical (Figure S3D; Table S2.11). Further, hypoxia (HP) preconditioning,⁶² which protects also against

IRI, also shows a strong overlap with the CR and AR-responsive gene sets (Figure 3G; Figure S3D; Table S2.11). Thus, CR and HP may both act to modify the sex profile of the kidney through AR-mediated signaling and the resulting outcome to kidney injury.

Single-nuclear multiomic profiling of AR function in the mammalian kidney

To obtain a more detailed insight into AR regulation in the nephron, we applied 10X multiomic single-nuclear RNA- and ATAC-seq profiling to examine chromatin regulation and aligned gene activity in wild-type (WT) and *Six2-Ar-KO* kidneys at 8–10 weeks of age (Figure 4A). Stringent quality control steps and depth normalization approaches were applied to minimize technical and batch effects. Data from individual samples were integrated, and nuclei were clustered based on both RNA and ATAC modalities. Clusters were manually annotated based on established cell-type markers (Figures S4A and S4B).

As expected, integrated RNA/ATAC data suggest molecular differences between sexes and genotypes predominantly manifest among PT cell clusters, where previous scRNA-seq studies¹⁹ have demonstrated sexually dimorphic gene activity predominantly maps to PT segments 2 and 3 (PT-S2 and PT-S3; Figure 4B). In the multiomic data, PT-S1 cluster comprised S1 cells from all genotypes and sexes, indicative of a low level of AR-dependent variability between male and female sexes (Figure 4B). By contrast, WT nuclei from PT-S2 and PT-S3 clustered separately comparing male and female kidney samples (Figures 4B and 4C). Further, the vast majority of male *Six2-Ar-KO* nuclei clustered with female WT and *Six2-Ar-KO* nuclei (Figures 4B and 4C). Analysis of the expression of top male- and female-specific markers distinguishing individual PT segments indicated male PT segments resemble their female counterparts following AR removal (Figure 4D). These data indicate that each PT segment adopts a distinct segmental identity, with a segment-specific female ground-state that is masculinized by the direct action of AR in response to androgens in the male kidney.

Using the single-nuclear RNA data, we identified a total of 1,035 F-biased and 736 M-biased genes (Figure 4E; Table S3.1; representing the “single-nuclear sex-biased genes”), where higher sequencing depth in female samples possibly inflated the number of F-biased genes. Of note, PT-S3 showed the highest number of sex-biased genes (Figure S4C). Upon AR removal in male nephrons, 220 F-biased genes were up-regulated among PT segments while 211

(B) PCA plot demonstrates the relative renal transcriptional profile of mice undergoing various treatment regimens. Sample variations were evaluated based on the expression of the core sex-biased genes. CM, castration in males; OF, ovariectomy in females; TES, transient testosterone administration; WT, wild type; KO, knockout.

(C) Heatmap shows the scaled average expression levels of the core set genes in male and female samples in individual treatments.

(D) Percentage of the core sex-biased genes that were perturbed in individual treatments are shown for male and female samples in bar plots. The number of genes that are perturbed in each treatment and the corresponding percentages are listed. Arrows indicate the direction of perturbation in gene expression as compared with controls.

(E) Stacked bars demonstrate the proportion of core sex-biased genes that are perturbed consistently in castration and nephron-specific AR knockout experiments in male samples. Pie charts show the percentage of AR-responsive genes that were perturbed in caloric restriction (CR) experiment.⁶²

(F) Scatter plot compares changes in the expression of core sex-biased genes in nephron-specific removal (*Six2-Ar-KO*) and systemic removal (*Sox2-Ar-KO*). (G) Venn diagrams showing the overlap of core set of sex genes responsive to both AR removal and CM compared with the following treatments: (1) TES, testosterone injection; (2) CR, caloric restriction; (3) HP, hypoxia; and (4) CR and HP.

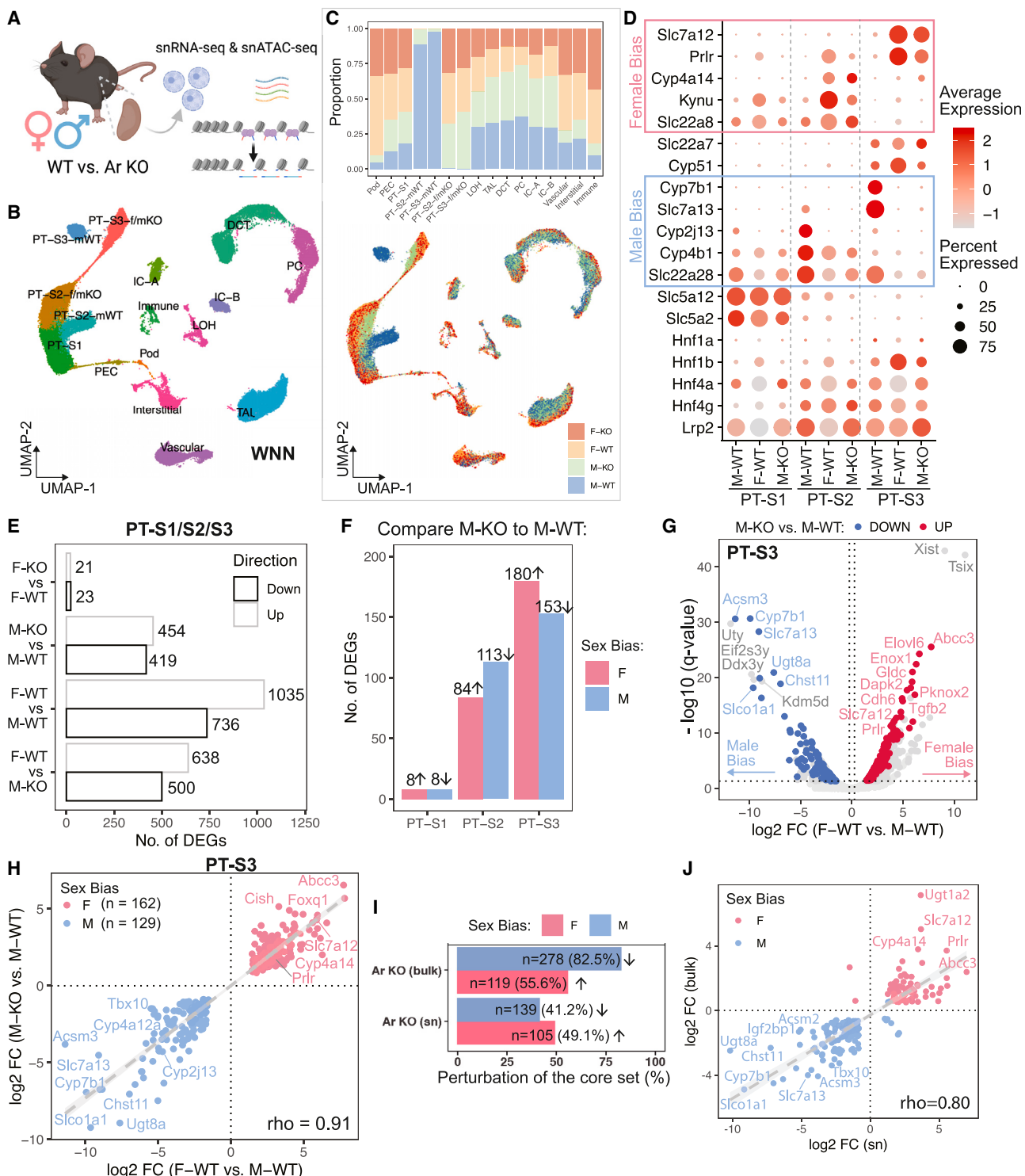


Figure 4. Single-nuclear multiomic profiling of AR function in the mammalian kidney

(A) Schematic summary of the single-nuclear multiomic experiment. Created with BioRender.com.

(B) UMAP plot indicates the divergent features between male and female PT cells, whereas the other cell populations co-cluster regardless of sex. Nuclei were clustered based on RNA and ATAC modalities using weighted nearest neighbor (WNN) graph.

(C) Distribution of sex and genotype among all cell populations shown in (B). Top, stacked bar plot shows composition in each cluster; bottom, nuclei in the UMAP plot (B) colored by different sex-genotype combinations.

(D) Dot plot demonstrates the expression pattern of top marker genes for individual PT segments. Known sex-biased genes are indicated.

(E) Bar plot shows the total number of differentially expressed genes identified using the multiomic RNA data by four pairwise comparisons within PT segments.

(legend continued on next page)

M-biased genes were down-regulated (Table S3.2; see Figure 4F for segment-specific quantification), which comprise a set of single-nuclear sex-biased genes with large effect sizes (Figure 4G; Figure S4F), but the expression of sex-chromosome genes was independent of AR. These AR-responsive sex-biased genes showed high concordance of relative gene expression in female WT and male KO PTs when compared with male WT (Spearman correlation rho = 0.91; Figure 4H; Figures S4G and S4H). The small number of gene expression changes observed on AR removal from female nephrons (21 genes up-regulated and 23 down-regulated) likely represent background rather than *bona fide* regulation (Figure 4E; Table S3.3). When we compared changes in expression before and after AR removal between bulk and single-nucleus RNA-seq experiments, we found that 41%–49% of the core sex-biased genes identified in bulk data (Figure 1B) were identified in the single-nuclear data (Figure 4I), which also show a high concordance in fold change (Spearman correlation rho = 0.80; Figure 4J).

Single-nuclear ATAC identified AR response elements near sex-biased genes

To further delineate the molecular mechanism of AR-directed regulation of dimorphic gene expression, we examined the chromatin landscape within each kidney cell type using the single-nuclear ATAC data, with a focus on PT cells (Figure 5A). Removal of Ar resulted in a pronounced co-clustering of Ar mutant male PT cells with WT and Ar mutant female PT cells, suggesting AR plays a major role in sex-biased regulation of chromatin accessibility in PT (Figure 5A). Global comparison of chromatin states between PT populations revealed that segment-specific differences are larger than sex-dependent differences within each segment (Figure S5A). We applied differential accessibility analysis between male and female WT nuclei to identify potential functional response elements that are proximal or distal to the AR-responsive genes (Table S4). Akin to sex-biased gene expression (Figure S4C), PT-S3 showed the highest number of differentially accessible regions (sex-biased differentially accessible regions (DARs); Figure 5B; Figure S5B): 7,987 F-biased peaks and 11,972 M-biased peaks, with 1,160 F-biased peaks and 1,087 M-biased peaks within 100 kb of the transcriptional start site (TSS) of genes with sex-biased expression (Table S3.4).

To examine AR-dependent sex-specific chromatin differences, we compared M-biased open and closed (the latter equivalent to F-biased open) DARs between M-WT and M-KO using F-WT as a common standard (Figure S5B; Table S4). Of the M-biased open peak set from S2 (11,079 peaks) and S3 (15,307 peaks), 83.1% of the S2 peaks and 66.7% of the S3 peaks showed a loss of differential accessibility comparing M-KO to F-WT in line with direct AR regulation of chromatin accessibility (Figure S5B). Examining the F-biased open peaks,

approximately half gained female-like accessibility on AR removal in the male kidney (Figure S5B).

For the AR-responsive sex-biased genes identified from the multiomic data (Figures 4F–4H; Figures S4F–S4H), we evaluated their chromatin state using gene accessibility score ψ (Figure 5C), a metric that quantifies the openness of a genomic region using a weighted sum of peaks within the gene body and promoter region (up to 5 kb upstream of its TSS). As expected, F-biased genes are preferentially open in female PTs, while M-biased genes are more open in male PTs (Figures 5C and 5D). Following AR removal from male nephrons, 98% of M-biased genes show decreased accessibility, especially in PT-S2 (Figures 5C and 5D; Table S3.5), while 97% of F-biased genes showed a more open chromatin profile, mostly prominent in PT-S3 (Figure 5D; Table S3.5). In male PT-S1, little effect was observed on either gene expression (Figure S4D) or chromatin status (Figure 5D) upon AR removal. Consistently, the most striking reduction in the DARs near AR-dependent down-regulated genes in M-KO was found in the M-biased open distal regions in PT-S2, and in those near AR-dependent up-regulated female genes in male-closed proximal regions (within 1 kb upstream of TSS) in PT-S2 (Figure 5E). For genes with an F-bias, Ar removal in the male kidney resulted in an increase in open chromatin in proximal and distal regions in both PT-S2 and PT-S3 (Figure 5E), consistent with the activation of an F-biased gene set (Figure 4G).

AR binding to chromatin associated with kidney target genes has been identified through ChIP-seq following acute testosterone administration injection.⁴⁶ To examine the AR-dependent transcription factor binding in the male open DARs regions compared with F-WT, we performed motif enrichment analysis on DARs associated with AR binding in the ChIP-seq experiments. This analysis showed a strong enrichment for predicted AR motifs in distal regions associated with *cis*-regulatory elements, as well as motifs for several other transcriptional regulators, notably Hnf1a/1b and Hnf4a/4g, which are broad regulators of PT programs (Figure 5F). Thus, PT-specific actions of Ar are likely to be directed by a broader PT gene regulatory program.

We also performed differential accessibility analysis between M-WT and M-KO nuclei (Table S3.6). Among the sex-biased DARs identified (Figure 5B), 167 F-biased peaks became more open upon AR removal in male PT-S3, while 211 M-biased peaks became more closed (Figure 5G; AR-responsive DARs). Notably, many of the AR-responsive DARs were near genes with the most marked sex-biased expression (see also Figures 4G and 4H). When AR-responsive PT-S3 DARs were compared with the AR ChIP-seq data,⁴⁶ we observed a 1.7-fold increase in AR binding among M-biased peaks than F-biased peaks (two-proportion z-test, p value = 4.3E–6), whereas Hnf4a binding did not show a significant difference

(F) Bar plot lists segment-wise number of single-nuclear sex-biased genes that were perturbed upon AR removal.

(G) Volcano plot shows single-nuclear sex-biased genes identified in PT-S3 segment, where genes that are perturbed by AR removal in the male kidney are highlighted.

(H) Scatter plot contrasts the effect of nephron-specific AR removal in male to the observed sex biases.

(I) Bar plot compares the percentage of the core sex-biased genes that were perturbed by nephron-specific AR removal, between bulk and single-nuclear RNA-seq.

(J) Scatter plot shows the impact of nephron-specific AR removal on common sex-biased gene, using bulk or single-nuclear RNA-seq data.

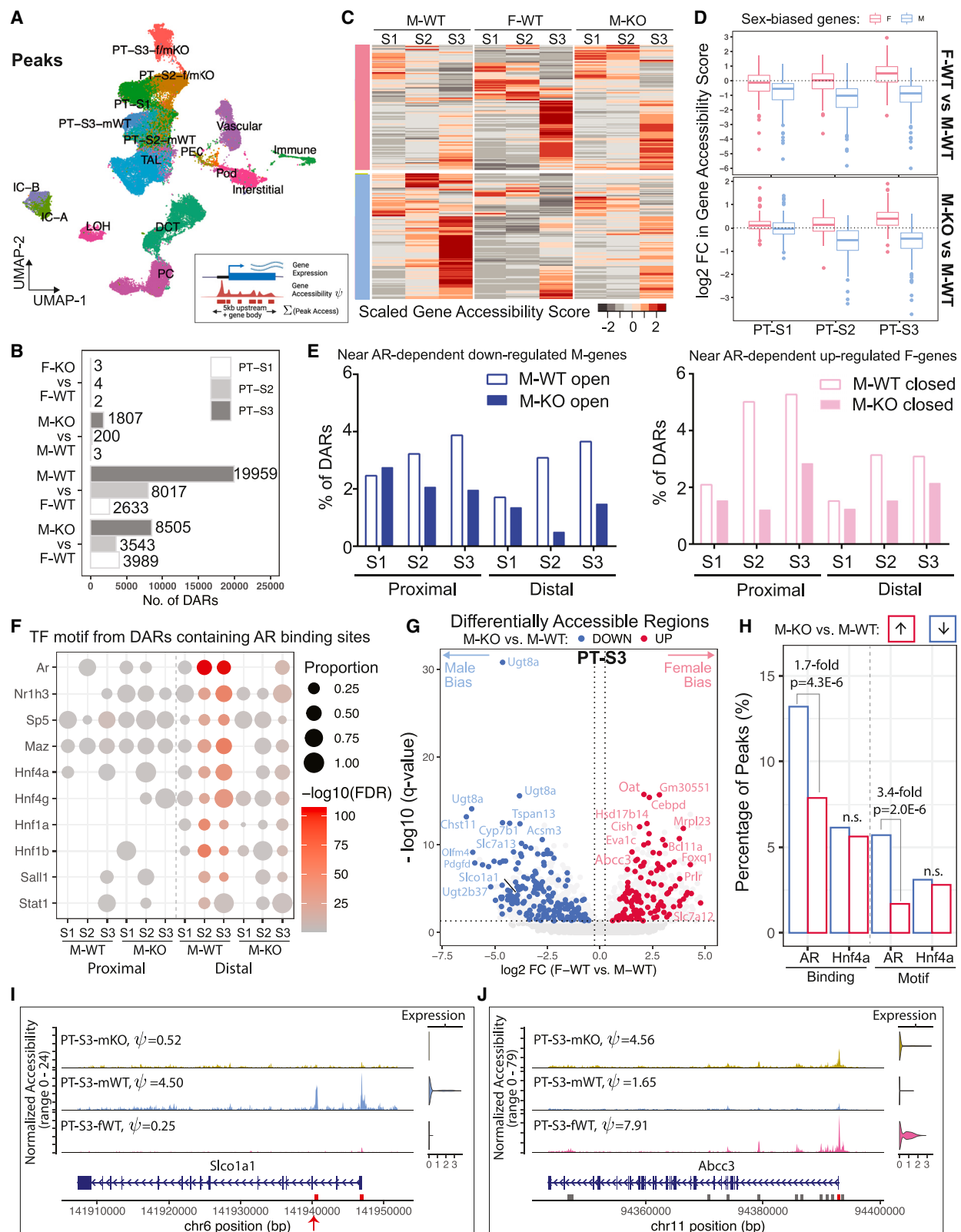


Figure 5. AR response elements are located near sex-biased genes

(A) UMAP plot shows clustering outcome using peaks called from the single-nuclear ATAC data. PT-S3-f/mKO, co-clustering of PT-S3 cells from F-WT, F-KO, and M-KO; PT-S2-f/mKO, co-clustering of PT-S2 cells from F-WT, F-KO, and M-KO; mWT, M-WT.

(legend continued on next page)

(Figure 5H). When compared with F-biased peaks, AR-responsive M-biased peaks showed an enrichment for AR motif (two-proportion z-test, p value = 2.0E-6), but not for the Hnf4a motif (Figure 5H). PT-S2 DARs behaved similarly, but none of the sex-biased DARs in PT-S1 were perturbed on AR removal (Figures S5D and S5E). Together, these data are consistent with direct AR regulation of *cis*-regulatory modules driving expression of male-enriched gene expression in the S2 and S3 segments of the PT.

To identify additional TFs that mediate the sex-biased transcription program, we performed TF motif enrichment analysis on sex-biased DARs within 100 kb of the TSS of the AR-responsive gene set (Figure S5C; Table S3.7). In addition to AR, M-biased DARs predicted motif enrichment in PT-S3 for Rfx3, a key factor in cilium biogenesis.⁶⁵ Motif recovery further highlighted the likely interface of AR action with general PT regulatory programs mediated by Hnf1a/b and Hnf4a/g which were enriched in both M- and F-biased DARs (Figure S5C; Table S3.7). F-biased DARs showed a strong motif enrichment for Stat5a/b and Bcl6 which lie downstream of prolactin and GH signaling^{66,67} suggesting alternative pathways of F-biased regulation (see discussion).

Integrating AR ChIP-seq⁴⁶ and our multiomic data, we were able to uncover putative AR response elements near sex-biased genes. For example, there were 5 M-biased DARs (2 proximal and 3 distal) annotated in the genomic region of *Sco1a1* in PT-S3 (Table S3.4), and 3 were preferentially closed in male PT-S3 when AR was removed (Table S3.6), including the intronic peak with AR binding site (Figure 5I), a phenomenon that was also found in PT-S2 (Figure S5F). Note that out of the 6 M-biased DARs (5 intronic and 1 in the promoter) with AR binding annotated in the genomic region of *Cyp2j13*, the promoter region peak was identified as the most significantly down-regulated post AR removal (false discovery rate [FDR] < 3.4E-5) (Figure S5G; Tables S3.4 and S3.6). In the genomic region of *Abcc3*, we detected 11 F-biased DARs (6 within the gene body and 5 distal) in PT-S3 (Table S3.4); one peak at the promoter was preferentially open in male PT-S3 without AR (Figure 5J), and another peak 53 kb upstream in between *Abcc3* and *Cacna1g* was bound by both AR and Hnf4a (Tables S3.4 and S3.6), suggesting multi-factor regulation of sex-biased gene expression. Collectively, examination of AR-responsive peaks

near candidate genes with AR binding information provided strong evidence for direct AR action mediating chromatin changes near M-biased genes in PT-S2 and S3, but not F-biased genes.

RNAscope validates dimorphic gene expression in proximal tubule

To visualize gene expression directly in PT segments, we combined uniquely labeled RNAscope probes and performed *in situ* hybridization to adult male and female kidney sections (Figure 6). M-biased gene *Cyp2j13* (a member of cytochromes P450 family, metabolizing arachidonic acid into epoxyeicosatrienoic acids for vasodilation and other functions⁶⁸) exhibited AR-dependent expression in PT-S2, colocalized with S2 marker *Cyp2e1* (Figure 6A). *Sco1a1* is the top candidate for AR-responsive M-biased gene (Figure 4H), which encodes solute carrier organic anion transporter polypeptide 1 (OATP1) important for the uptake of steroid conjugates and prostaglandin E2 into the cell.^{69,70} As predicted, *Sco1a1* mRNA was highly male-specific among PT-S2, and entirely absent upon AR removal from male nephrons (Figure 6B). M-biased *Atp11a* encodes phospholipid-transporting ATPase IH, an integral membrane P4-ATPase that function as flippases at the plasma membrane to translocate phospholipid from the outer to the inner leaflet.⁷¹ *Atp11a* expression was M-biased in PT-S2 and PT-S3; total mRNA in individual PT cells recapitulated single-cell measurement (Figure 6C). Interestingly, *Atp11a* mRNA was abundant in the cytoplasm of male PT-S2 and PT-S3 but was concentrated in the nuclei among female PTs as well as among male PT cells without AR (Figure 6C). Phospholipid-transporting ATPase IH is reported to be actively translated only in male PTs, where phospholipid asymmetry across the cell membrane regulates solute transport and membrane protein function.^{72,73}

The F-biased gene *Gsta4* (glutathione S-transferase alpha 4), which is known to protect against oxidative injury and renal fibrosis⁷⁴, was highly differentially expressed in female PT-S2 and induced in the male PT-S2 segment on AR removal (Figure 6A). The top F-biased gene *Abcc3* (or *Mrp3*) encodes a member of the superfamily of ATP-binding cassette (ABC) transporters, essential for the efflux of organic anions, including steroid conjugates, glutathione conjugates, and prostaglandin J2.⁷⁵ *Abcc3* showed female-specific expression

(B) Bar plot shows the number of sex-biased differentially accessible regions (DARs) in PT segments identified for each pairwise comparison (absolute log₂FC > 0.25, adjusted p value < 0.05).

(C) Schematic summary of the computation of gene accessibility score ψ and heatmap shows the scaled gene accessibility score ψ for AR-responsive genes in M-WT, F-WT, and M-KO PT segments.

(D) Box plots demonstrate fold change in gene accessibility score ψ of AR-responsive genes within individual PT segments.

(E) Histograms showing the percentage of the proximal and distal DARs from M-WT and M-KO compared with F-WT that were nearby AR-dependent down-regulated M-biased (blue) and up-regulated F-biased (pink) genes.

(F) Dot plot summarizes TF motif enrichment in the open DARs containing AR binding sites based on the published ChIP-seq dataset⁴⁶ in M-WT and M-KO compared with F-WT PT segments.

(G) Volcano plot shows DARs within 100 kb of sex-biased genes in PT-S3. 11,972 peaks were differentially open in male (left) and 7,987 peaks were differentially open in female (right). We colored F-biased peaks that are preferentially open in M-KO in red and M-biased peaks that are preferentially closed in M-KO in blue. Each dot represents a 500-bp region, where the nearest gene is annotated.

(H) Bar plot shows the prevalence of TF binding and motif among PT-S3 sex-biased DARs that were altered by AR removal. TF binding was based on ChIP-seq data in the mouse kidney.⁴⁶ TF motif position weight matrices (PWMs) were retrieved from the Jasper database⁶⁴ for AR (MA0007.3) and Hnf4a (MA0114.3).

(I and J) Coverage plots of two representative sex-biased genes, *Sco1a1* (M-biased; I) and *Abcc3* (F-biased; J). All peaks called in the region are shown in gray boxes, where DARs are highlighted in red. Peaks with potential AR binding site are indicated by red arrows.

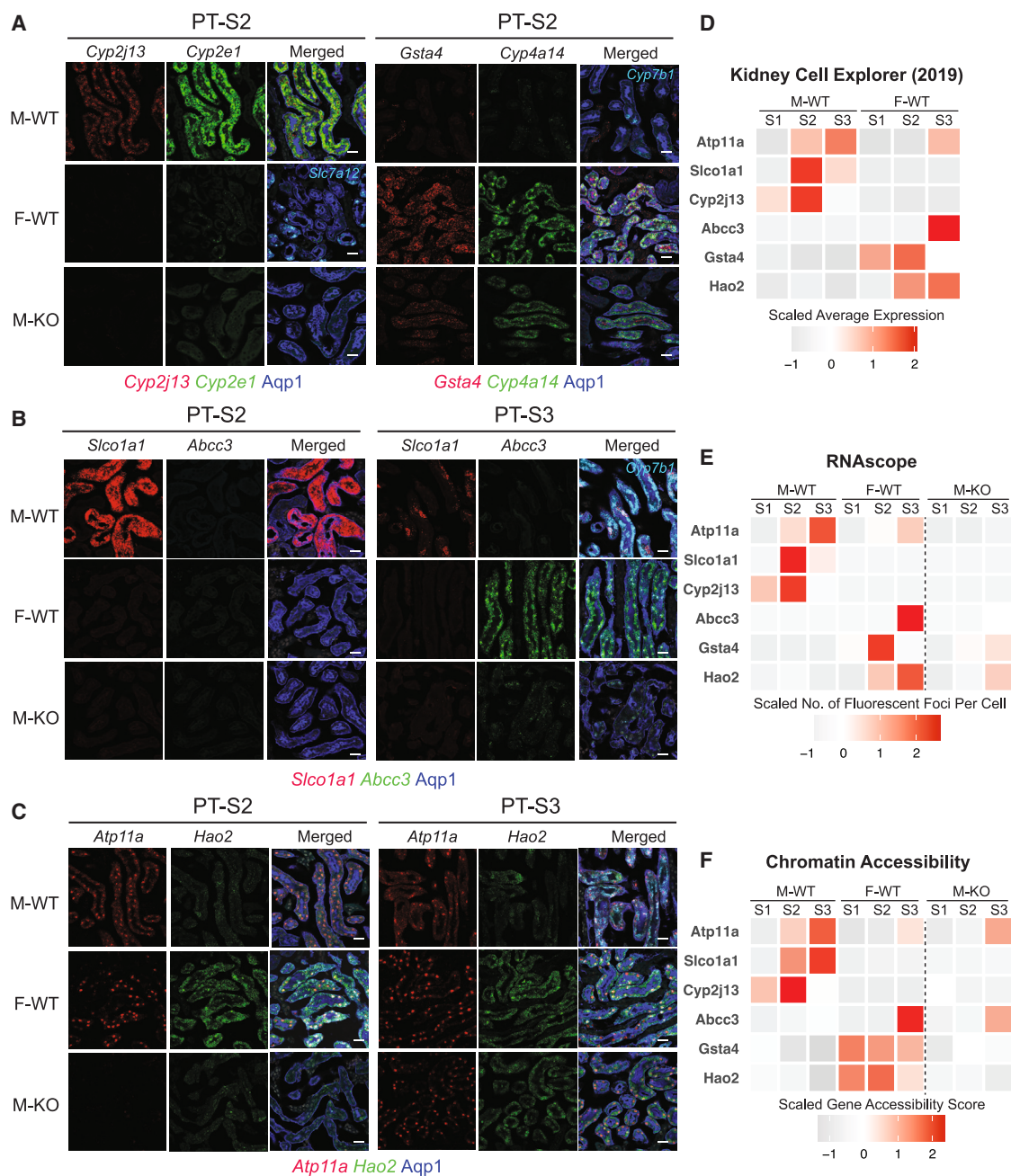


Figure 6. Fluorescence RNA *in situ* hybridization by RNAscope validates dimorphic gene expression in proximal tubule

(A–C) RNAscope assay directly visualized the expression levels of sex-biased genes in M-WT, F-WT, and M-KO PT-S2 and S3 (scale bars, 20 μ m): co-stained with an antibody against Aqp1 (blue) demarcating the PT. (A) Left, *Cyp2j13* (red) and *Cyp2e1* (green, male PTS2 marker) co-stained with *Slc7a12* (cyan, female PTS2 marker); right, *Gsta4* (red) and *Cyp4a14* (green, female PTS2 marker) co-stained with *Cyp7b1* (Cyan, male PTS3 marker). (B) *Slco1a1* (red) and *Abcc3* (green), co-stained with *Cyp7b1* (cyan, male PTS3 marker). (C) *Atp11a* (red) and *Hao2* (green).

(D–F) Tile maps show the expression and chromatin profile of top sex-biased genes in M-WT and F-WT PT segments: (D) data from previous scRNA-seq experiment¹⁹, (E) *in situ* expression of top sex-biased genes measured by RNAscope, and (F) the estimated chromatin accessibility.

in PT-S3 comparing male and female kidneys and a striking, though partial, up-regulation upon AR removal from male nephrons (Figure 6B). In addition, the F-biased gene *Hao2* encodes peroxisomal hydroxy acid oxidase 2, which was shown to eliminate lipid accumulation and inhibit progression of clear cell renal cell carcinoma.^{76,77} *Hao2* was highly expressed in fe-

male PT-S2 and PT-S3, but only low levels of expression were detected in homologous male PT segments (Figure 6C); a marked increase in PT-S3 *Hao2* expression was observed on AR removal from the male nephrons (Figure 6C). Together, RNAscope experiment validated the expression pattern of candidate AR-responsive sex-biased genes in PT segments,

Developmental Cell

Article

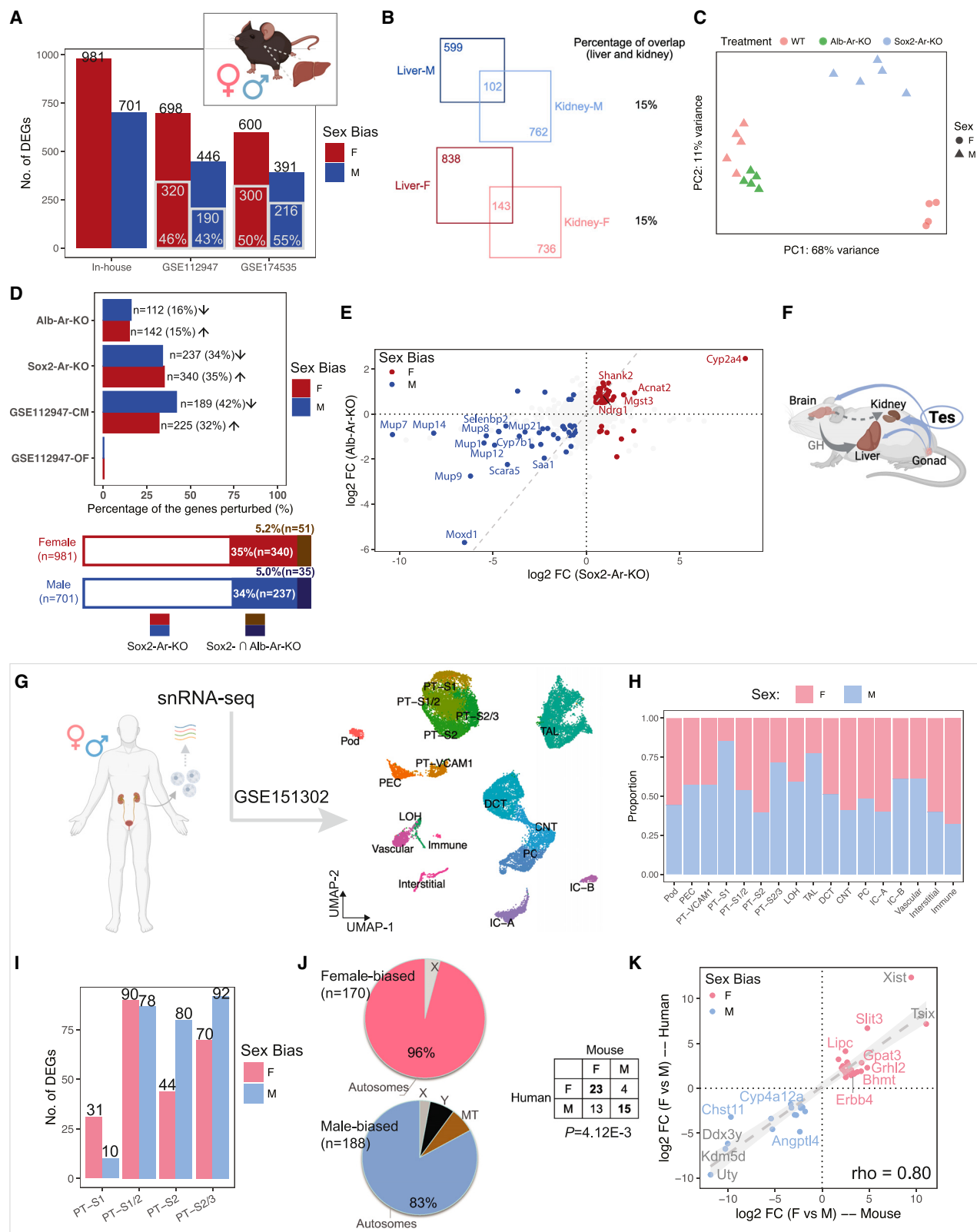


Figure 7. Distinct and shared processes of dimorphic gene expression between organs and species

(A) Bar plot shows the number of liver sex-biased genes identified in this study (in-house) and those reported in the literature. Gray-contoured bars indicate the number of genes overlapping with the in-house list.

(legend continued on next page)

as predicted by sequencing results (Figures 6D and 6E). Further, we found that the chromatin accessibility profile of these candidate genes was also largely in line with the expression pattern (Figure 6F).

Distinct and shared processes of dimorphic gene expression in the kidney and liver

In contrast to the kidney, the liver has been shown to be regulated by sex-dependent dynamics of GH stimulation, where GH release by the hypothalamus-pituitary axis is under direct androgen and estrogen control.^{78,79} However, to our knowledge, the effects of direct AR removal from hepatocytes on sexually dimorphic expression in the liver have not been addressed. To compare liver and kidney mechanisms, we initially identified a total of 1,682 genes with sex-biased gene expression in the C57BL/6 mouse liver at 8–12 weeks through bulk RNA-seq (Figure 7A; Table S5.1), 43%–55% of which were shared with two previous studies^{80,81} (GSE174535 and GSE112947) (Figure 7A). The concordance of expression profile between datasets was high (Spearman correlation rho = 0.92–0.93; Figure S7B). Comparing sex-biased genes in the liver and kidney, we identified 102 shared M-biased genes (15%) and 143 shared F-biased genes (15%) (Figure 7B), a significant conservation of sex differences between the liver and kidney (chi-squared test; p value = 2.2E–16), when compared with genes shared across sexes in the two organs (5%).

To investigate the role of AR in the mouse liver, we compared hepatocyte-specific removal of *Ar* with an albumin CRE strain⁸² (Alb-Ar-KO) to systemic removal (Sox2-Ar-KO). As expected, PCA analysis across perturbations showed systemic AR removal had a more dramatic effect than hepatocyte-specific removal (Figures 7C and 7D). Systemic AR removal resulted in the down-regulation of 34% of genes with M-biased expression and up-regulation of 35% of those with F-biased gene expression (Figure 7D; Table S5.2), consistent with previously reported castration experiments⁸⁰ (Figures S7C and S7D). By contrast, 15%–16% of sex-biased genes were perturbed on hepatocyte-specific AR removal, in directions consistent with male/female biases (Figure 7D; Table S5.3). 5% of genes with liver sex biases in expression were shared between the systemic and hepatocyte-specific AR removal (Figure 7D). Further, the magnitude of expression changes was greater for systemic AR removal (Figure 7E), with a particularly marked alteration in the expression of genes encoding major urinary proteins (*Mup1/7/8/9/12/14/21*) and cytochrome P450 member (*Cyp2a4*). We did not detect a high concordance between systemic and hepatocyte-specific AR removal (Spearman correlation, rho = 0.39; Fig-

ure 7E), indicating the indirect action of AR controlling sex-specific gene expression in hepatocytes: a moderate perturbation was observed following AR removal in hepatocytes to a small number of genes sharing sex-biased expression in the liver and kidney. Only a handful of genes were predicted to share direct AR control of their expression in these two organs, including *Cyp7b1*, *Selenbp2*, *Cyp4a12a*, and *Oat* (Table S5.4).

Conserved renal sex differences in the human and mouse

Several reports have documented human kidney-associated differences in gene expression between the sexes.^{83–85} To determine whether conserved mechanisms extend from the mouse to the human kidney, we re-analyzed bulk RNA-seq data on kidney biopsies from adult male and female donors (GTEx v8⁸⁴). These studies showed only a modest number of genes differentially expressed between the sexes in human, 1 F-biased gene (*KDM5C*, X-linked) and 73 M-biased genes (2 X-linked, 63 Y-linked, and 8 autosomal). The three conserved sex-biased genes comparing mouse (both the core and full set; Figure 1B; Table S6) and human data are all encoded by the Y chromosome: *UTY*, *DDX3Y*, and *KDM5D*.

Examining recent single-nuclear RNA-seq dataset for the human kidney (2 female and 3 male donors; GSE151302⁸⁶; Figure 7G) showed co-clustering of expression data for male and female PT segments with no apparent sex bias in cluster composition (Figure 7H). Differential gene expression analysis uncovered a total of 170 F- and 188 M-biased genes, over 80% of which are autosomal (Figures 7I and 7J; Table S6). Through ortholog matching, we identified 23 F-biased genes and 15 M-biased genes with conserved expression between the human and mouse kidney (Figure 7K; Fisher's exact test, p value = 4.12E–3), including predicted AR-responsive genes in the murine kidney (*Chst11* and *Bhmt*; Tables S2 and S3) and murine kidney and liver (*Cyp4a12a*; Table S5.4). Though there are several caveats with these human studies (see discussion), these findings suggest a limited conservation in sex-biased expression and AR-mediated in-organ regulation between the mouse and human kidney.

DISCUSSION

In this study, we used time course bulk RNA-seq and single-nuclear multiomic data to investigate the regulatory mechanism of renal sexual dimorphic gene expression in mice. Sexually dimorphic gene expression in PT cells is established under gonadal

(B) Venn diagrams show the number of sex-biased genes that are shared in the kidney and liver.
(C) PCA plot demonstrates the impact of hepatocyte-specific (Alb-Ar-KO) and systemic AR removal (Sox2-Ar-KO), as compared with WT samples.
(D) The percentage of in-house liver sex-biased genes that were perturbed in individual treatments is shown in the bar plot (top) and stacked bar plot (bottom). Arrows indicate the direction of perturbation in gene expression when compared with controls.
(E) Scatter plots compare the changes in expression of in-house liver sex-biased genes between systemic and hepatocyte-specific AR removal. The dashed gray diagonal line marks equal impact.
(F) A schematic summary of how testosterone influences the sexual dimorphism in the kidney and liver. Created with BioRender.com.
(G) UMAP plot shows clustering of human renal single-nuclear RNA-seq data (GSE151302).
(H) Composition of male and female cells in each cluster in (B).
(I) Bar plot shows the number of sex-biased genes among each PT cluster in (B).
(J) Pie charts demonstrates the percentage of autosomal versus X/Y-linked genes among all the sex-biased genes identified in (D).
(K) Comparison of sex-biased gene expression in human and mouse kidney reveals conserved sexual dimorphism. The table lists the number of orthologs that show sex biases in gene expression; the scatter plot shows the differences in expression of common sex-biased genes in human and mouse PT segments.

Developmental Cell

Article



control between 4 to 8 weeks postpartum primarily through androgen signaling, and ovary removal and *Esr1* deletion had little effect. Several lines of evidence support a direct regulatory action of AR binding to chromatin within *cis*-regulatory regions of genes showing M-biased expression as a major driver of sexually dimorphic gene expression in the mouse kidney. Critically, AR activity in PT cells is required for establishing a normal male program of gene expression. The requirement correlates with androgen responsiveness of M-biased genes, and AR motif enrichment and ChIP-seq binding studies, that point to AR engagement within distal regulatory regions of genes with M-biased expression. Co-recovery of motifs for general regulators of PT identity and cell function (*Hnf1a*, *Hnf1b*, *Hnf4a*, *Hnf4g*) suggests AR acts in conjunction with broader PT regulatory mechanisms.

Although there is strong evidence for a direct activating role for AR in controlling M-biased genes, the mechanisms regulating F-biased gene expression are less clear. Loss of AR in PT cells results in a substantial ectopic activity of F-biased genes indicating that suppression of the female program is dependent on direct AR activity in PT cells. However, we did not observe a strong enrichment of AR motifs in distal regulatory regions around the F-biased gene set suggesting an indirect regulatory role; for example, transcriptional activation of a gene encoding a repressor of the female program. The F-biased program is also associated with motif predictions from DARs for *Stat5a*, *Stat5b*, and *Bcl6*, a negative regulator of Stat action.⁴¹ Interestingly, both male and female patterns of sexually dimorphic gene expression in the mouse liver are controlled through GH signaling to hepatocytes,⁴⁴ though our analysis of hepatocyte removal of *Ar* suggests a minor role for direct AR action (see below). These findings raise the possibility of direct GH control of the F-biased kidney program. *KidneyCellExplorer*¹⁹ (<https://cello.shinyapps.io/kidneycellexplorer/>) shows GH receptor is specifically expressed in male and female PT cells consistent with a GH input. In addition, prolactin, the peptide hormone controlling postnatal functions such as milk production, is related to GH and acts through its receptor (*Prlr*) to control *Stat5a*- and *Stat5b*-directed transcription. *Prlr* shows one of the strongest biases in female enriched expression, consistent with prolactin signaling modulating female programs of kidney gene expression in association with reproduction. These observations argue for future studies focused on additional roles for GH-*Stat5a/Stat5b* and prolactin-*Stat5a/Stat5b* regulation of female kidney programs.

Functionally, sex-biased genes are involved in multiple biological pathways, most notably peroxisomal lipid metabolism in the male and NR pathways in the female. PTs utilize fatty acid as their major source of energy,⁸⁷ which is indispensable for their function in salt and water reabsorption.²² Peroxisomes oxidize long-chain fatty acids, whereas mitochondria break down short- or medium-sized fatty acids.⁸⁸ The bias for peroxisomal lipid metabolism possibly implies a higher energy demand in male PTs than in female,⁸⁹ together with increased lipid deposition in the cortex.⁸⁷ In time of shortage in energy or oxygen (i.e., ischemia), it would be necessary to remodel renal expression profile toward a more energy-conserving state, which could explain the transient reversal of male phenotype during CR⁶² and short-term fasting.⁹⁰ Moreover, a byproduct of beta-oxida-

tion is reactive oxygen species (ROS) produced by acyl-coenzyme A oxidases, which require antioxidant enzymes to neutralize. Excessive ROS due to high-energy state or reperfusion might contribute to chronic renal damage.⁹¹ On the other hand, F-biased program highlight lipid clearance and anti-oxidation. F-biased genes *Abcc3* and *Gsta2/4/5* are all involved in the NRF2 pathway, whose activation acts against oxidative stress⁹² and inflammation⁹³ to facilitate female resilience to kidney injury.⁹⁴

AR-mediated gene expression is not only involved in the transport of organic anions (e.g., steroid conjugates and prostaglandins) and other solutes across the plasma membrane but also directs cellular energetics and promotes lipid oxidation (see above) via *Ppara* and *Nr1h4/FXR*, both of which are nutrient-sensing TFs important for ciliogenesis in PTs.⁹⁵ Moreover, AR has also been shown to play a critical role in regulating mitochondrial activities,⁹⁶ stressing the connection between AR-mediated signaling and cellular energetics. This link between AR-dependent gene regulation and high-energy state to support renal function indicates how AR-mediated signaling could undermine renal function chronically, a potential cause for the M-biased susceptibility to kidney diseases. Interestingly, analysis of gene expression in published datasets of male mice undergoing 4-week CR highlighted a pronounced loss of AR-responsive gene expression, feminization of the male kidney, and a conferred resilience to acute kidney injuries.⁶² CR has been reported to lower testosterone levels,^{97,98} which likely accounts for these observations and raises new questions about the complexity of actions on organ activity following an alteration of metabolism. A similar analysis of renal-protective HP conditioning suggests a shared link with CR to AR-responsive gene sets suggesting sexual dimorphic gene activity may underlie multiple conditioning regimen.

In the liver, hypothalamus-pituitary-directed pulsatile GH release dominate dimorphic gene expression in the liver^{39,41,99,100} though our study shows 16% of M-biased genes in the liver were perturbed after adipocyte-specific removal of AR. The contrasting regulatory mechanisms of sexual dimorphism in the kidney and liver (see also Sundseth and Waxman¹⁰¹) suggests that sexual differentiation of the two organs might have evolved separately and been selected for by different forces. Primarily functioning as a biochemical organ, the liver needs to respond to fluctuation in energy supply and to coordinate its enzymatic reactions to animal behaviors (e.g., food intake and physical activity).¹⁰² Direct link to the hypothalamus and pituitary can couple liver function to circadian/ultradian rhythms and fine-tune its action from hour to hour (a single GH pulse can alter *Bcl6* expression⁴¹), as seen in the thyroid and adipose tissue.¹⁰³ By contrast, the functions of the kidney are fundamentally biophysical¹⁰⁴—ultrafiltration and osmotic regulation¹⁰⁵—where autoregulation is prevalent.¹⁰⁶ Androgens could reinforce the energetic profile of the kidney, but likely over a slightly longer timescale. In this regard, sexual differentiation of the kidney and liver plausibly allowed for adaptation to distinct environmental challenges during evolution.

Regarding renal sex differences in the human kidney, published analyses so far have not demonstrated extensive dimorphic expression, beyond the X and Y chromosomes, as reported

here in the mouse PT.^{84,86,107,108} Limitations in variable sample quality and variation among individuals sampled is a confounding factor in the human studies. The full scope of human renal (and other organ) sex differences awaits further investigation. However, our re-analysis of human data revealed limited sex-dependent expression programs in the human kidney, with a modest conservation between human and mouse, lending support to a comparative approach^{109,110} to study the molecular mechanism of sex differences in renal physiology and disease modeling.

The observation that mammalian organs differ between the sexes raises mechanistic questions as to how and why and to the implications for those differences in organ function and disease. Our study here addressed the developmental question of how sexual diversity is regulated contrasting the kidney with the liver, indicating different mechanisms at play, and comparing across evolution from mouse to human. We establish intriguing links of AR-regulated renal sexual dimorphism to disease phenotypes through pathway analysis showing that CR and HP conditioning, both approaches that mitigate IRI, feminize the male mouse kidney profile, suggesting a model that the action of these conditioning routines may be at least in part through differential expression of sexually dimorphic genes. More genetic studies are to be done to address the pathophysiology of sex-specific health disparities in kidney diseases.

Limitations of the study

The observation that mammalian organs differ between the sexes raises mechanistic questions as to how and why, and the role of sex differences in organ function and disease. Our study focused on the developmental question of the underlying regulation of sexual diversity in gene activity in the mouse kidney. The functional significance and pathophysiological implications of sexual dimorphism are open questions, though the connections between renal-protective preconditioning regimens and feminization of kidney gene expression in males are intriguing. Further, a deeper understanding of mouse and human conservation will require more extensive profiling of normal human kidneys.

STAR★METHODS

Detailed methods are provided in the online version of this paper and include the following:

- **KEY RESOURCES TABLE**
- **RESOURCE AVAILABILITY**
 - Lead Contact
 - Materials Availability
 - Data and Code Availability
- **EXPERIMENTAL MODEL AND STUDY PARTICIPANT DETAILS**
 - Husbandry conditions of experimental animals
 - Housing conditions of experimental animals
- **METHOD DETAILS**
 - RNA-seq
 - Single-nucleus multimodal experiment
 - Fluorescence RNA in situ hybridization
- **QUANTIFICATION AND STATISTICAL ANALYSIS**

- Bulk RNA-seq Data Analysis
- Isoform analysis
- Functional Inference
- Computational prediction of upstream regulators
- Single-nuclear multimodal data processing
- Single-nucleus multimodal differential analysis
- Gene accessibility score
- Motif Analysis
- ChIP-seq data processing

SUPPLEMENTAL INFORMATION

Supplemental information can be found online at <https://doi.org/10.1016/j.devcel.2023.08.010>.

ACKNOWLEDGMENTS

The authors thank members of the McMahon laboratory for helpful comments on experimental design and members of the Kim laboratory for useful discussion on single-cell analyses. We thank Dr. Ron Korstanje for orientating us to, and sharing data from, his groups analysis of multiple organs in a diversity outbred cross. Work in A.P.M.'s laboratory is supported by a grant from the National Institutes of Health (R01 DK126925). A.L.M. acknowledges support from the National Institutes of Health (R35GM143019) and the National Science Foundation (DMS2045327).

AUTHOR CONTRIBUTIONS

A.P.M. conceived the study. Funding support was generated by A.P.M., J.K., and L.P. Data were collected by J.L., K.K., and J.-J.G. and analyzed by L.X., J.L., S.Y.H., M.R., Z.M., F.G., and I.B.H. in consultation with A.P.M., A.L.M., J.K., and L.P. L.X., J.L., and A.P.M. wrote the manuscript incorporating comments from all participants.

DECLARATION OF INTERESTS

The authors declare no competing interests.

INCLUSION AND DIVERSITY

We support inclusive, diverse, and equitable conduct of research.

Received: May 5, 2023

Revised: July 20, 2023

Accepted: August 4, 2023

Published: September 5, 2023

REFERENCES

1. Carrero, J.J., Hecking, M., Chasnay, N.C., and Jager, K.J. (2018). Sex and gender disparities in the epidemiology and outcomes of chronic kidney disease. *Nat. Rev. Nephrol.* **14**, 151–164. <https://doi.org/10.1038/neph.2017.181>.
2. Kattah, A.G., and Garovic, V.D. (2020). Understanding sex differences in progression and prognosis of chronic kidney disease. *Ann. Transl. Med.* **8**, 897. <https://doi.org/10.21037/atm.2020.03.62>.
3. Aufhauser, D.D., Jr., Wang, Z., Murken, D.R., Bhatti, T.R., Wang, Y., Ge, G., Redfield, R.R., III, Abt, P.L., Wang, L., Svoronos, N., et al. (2016). Improved renal ischemia tolerance in females influences kidney transplantation outcomes. *J. Clin. Invest.* **126**, 1968–1977. <https://doi.org/10.1172/JCI84712>.
4. Neugarten, J., and Golestaneh, L. (2018). Female sex reduces the risk of hospital-associated acute kidney injury: a meta-analysis. *BMC Nephrol.* **19**, 314. <https://doi.org/10.1186/s12882-018-1122-z>.

Developmental Cell

Article



5. Hosszu, A., Fekete, A., and Szabo, A.J. (2020). Sex differences in renal ischemia-reperfusion injury. *Am. J. Physiol. Renal Physiol.* 319, F149–F154. <https://doi.org/10.1152/ajprenal.00099.2020>.
6. Smadel, J.E., and Swift, H.F. (1941). Experimental nephritis in rats induced by injection of antikidney serum: V. Chronic nephritis of insidious development following apparent recovery from acute nephrotoxic nephritis. *J. Exp. Med.* 74, 345–358. <https://doi.org/10.1084/jem.74.4.345>.
7. György, P., Seifter, J., Tomarelli, R.M., and Goldblatt, H. (1946). Influence of dietary factors and sex on the toxicity of carbon tetrachloride in rats. *J. Exp. Med.* 83, 449–462. <https://doi.org/10.1084/jem.83.6.449>.
8. Yabuki, A., Suzuki, S., Matsumoto, M., and Nishinakagawa, H. (1999). Sexual dimorphism of proximal straight tubular cells in mouse kidney. *Anat. Rec.* 255, 316–323. [https://doi.org/10.1002/\(SICI\)1097-0185\(19990701\)255:3<316::AID-AR7>3.0.CO;2-5](https://doi.org/10.1002/(SICI)1097-0185(19990701)255:3<316::AID-AR7>3.0.CO;2-5).
9. Yabuki, A., Suzuki, S., Matsumoto, M., and Nishinakagawa, H. (2003). Effects of sex hormones on the development of giant lysosomes in the proximal tubules of DBA/2Cr mouse kidney. *J. Anat.* 202, 445–452. <https://doi.org/10.1046/j.1469-7580.2003.00173.x>.
10. Neugarten, J., Kasiske, B., Silbiger, S.R., and Nyengaard, J.R. (2002). Effects of sex on renal structure. *Nephron* 90, 139–144. <https://doi.org/10.1159/000049033>.
11. Tahaei, E., Coleman, R., Saritas, T., Ellison, D.H., and Welling, P.A. (2020). Distal convoluted tubule sexual dimorphism revealed by advanced 3D imaging. *Am. J. Physiol. Renal Physiol.* 319, F754–F764. <https://doi.org/10.1152/ajprenal.00441.2020>.
12. Harris, A.N., Lee, H.-W., Osis, G., Fang, L., Webster, K.L., Verlander, J.W., and Weiner, I.D. (2018). Differences in renal ammonia metabolism in male and female kidney. *Am. J. Physiol. Renal Physiol.* 315, F211–F222. <https://doi.org/10.1152/ajprenal.00084.2018>.
13. Layton, A.T., and Sullivan, J.C. (2019). Recent advances in sex differences in kidney function. *Am. J. Physiol. Renal Physiol.* 316, F328–F331. <https://doi.org/10.1152/ajprenal.00584.2018>.
14. Li, J., Hatano, R., Xu, S., Wan, L., Yang, L., Weinstein, A.M., Palmer, L., and Wang, T. (2017). Gender difference in kidney electrolyte transport. I. Role of AT_{1a} receptor in thiazide-sensitive $Na^+ - Cl^-$ cotransporter activity and expression in male and female mice. *Am. J. Physiol. Renal Physiol.* 313, F505–F513. <https://doi.org/10.1152/ajprenal.00087.2017>.
15. Rinn, J.L., Rozowsky, J.S., Laurenzi, I.J., Petersen, P.H., Zou, K., Zhong, W., Gerstein, M., and Snyder, M. (2004). Major molecular differences between mammalian sexes are involved in drug metabolism and renal function. *Dev. Cell* 6, 791–800. <https://doi.org/10.1016/j.devcel.2004.05.005>.
16. Si, H., Banga, R.S., Kapitsinou, P., Ramaiah, M., Lawrence, J., Kambhampati, G., Gruenwald, A., Bottinger, E., Glicklich, D., Tellis, V., et al. (2009). Human and murine kidneys show gender- and species-specific gene expression differences in response to injury. *PLoS One* 4, e4802. <https://doi.org/10.1371/journal.pone.0004802>.
17. Veiras, L.C., McFarlin, B.E., Ralph, D.L., Buncha, V., Prescott, J., Shirvani, B.S., McDonough, J.C., Ha, D., Giani, J., Gurley, S.B., et al. (2020). Electrolyte and transporter responses to angiotensin II induced hypertension in female and male rats and mice. *Acta Physiol. (Oxf.)* 229, e13448. <https://doi.org/10.1111/apha.13448>.
18. Torres-Pinzon, D.L., Ralph, D.L., Veiras, L.C., and McDonough, A.A. (2021). Sex-specific adaptations to high-salt diet preserve electrolyte homeostasis with distinct sodium transporter profiles. *Am. J. Physiol. Cell Physiol.* 321, C897–C909. <https://doi.org/10.1152/ajpcell.00282.2021>.
19. Ransick, A., Lindström, N.O., Liu, J., Zhu, Q., Guo, J.-J., Alvarado, G.F., Kim, A.D., Black, H.G., Kim, J., and McMahon, A.P. (2019). Single-cell profiling reveals sex, lineage, and regional diversity in the mouse kidney. *Dev. Cell* 51, 399–413.e7. <https://doi.org/10.1016/j.devcel.2019.10.005>.
20. Chen, L., Chou, C.-L., Yang, C.-R., and Knepper, M.A. (2023). Multiomics analyses reveal sex differences in mouse renal proximal subsegments. *J. Am. Soc. Nephrol.* 34, 829–845. <https://doi.org/10.1681/ASN.0000000000000089>.
21. Verschuren, E.H.J., Castenmiller, C., Peters, D.J.M., Arjona, F.J., Bindels, R.J.M., and Hoenderop, J.G.J. (2020). Sensing of tubular flow and renal electrolyte transport. *Nat. Rev. Nephrol.* 16, 337–351. <https://doi.org/10.1038/s41581-020-0259-8>.
22. Yu, A.S.L., Chertow, G.M., Luyckx, V.A., Marsden, P.A., Skorecki, K., and Taal, M.W. (2020). *Brenner and Rector's the Kidney*, Eleventh Edition (Elsevier).
23. Koenig, H., Goldstone, A., Blume, G., and Lu, C.Y. (1980). Testosterone-mediated sexual dimorphism of mitochondria and lysosomes in mouse kidney proximal tubules. *Science* 209, 1023–1026. <https://doi.org/10.1126/science.7403864>.
24. Sabolić, I., Asif, A.R., Budach, W.E., Wanke, C., Bahn, A., and Burckhardt, G. (2007). Gender differences in kidney function. *Pflugers Arch.* 455, 397–429. <https://doi.org/10.1007/s00424-007-0308-1>.
25. Franco-Acevedo, A., Echavarria, R., and Melo, Z. (2021). Sex differences in renal function: participation of gonadal hormones and prolactin. *Endocrines* 2, 185–202. <https://doi.org/10.3390/endocrines2030019>.
26. Quan, A., Chakravarty, S., Chen, J.-K., Chen, J.-C., Loleh, S., Saini, N., Harris, R.C., Capdevila, J., and Quigley, R. (2004). Androgens augment proximal tubule transport. *Am. J. Physiol. Renal Physiol.* 287, F452–F459. <https://doi.org/10.1152/ajprenal.00188.2003>.
27. Loh, S.Y., Giribabu, N., and Salleh, N. (2017). Effects of gonadectomy and testosterone treatment on aquaporin expression in the kidney of normotensive and hypertensive rats. *Exp. Biol. Med. (Maywood)* 242, 1376–1386. <https://doi.org/10.1177/1535370217703360>.
28. Lattimer, J.K. (1942). The action of testosterone propionate upon the kidneys of rats, dogs and men. *J. Urol.* 48, 778–794. [https://doi.org/10.1016/S0022-5347\(17\)70768-9](https://doi.org/10.1016/S0022-5347(17)70768-9).
29. Hsu, Y.-J., Dimke, H., Schoeber, J.P.H., Hsu, S.-C., Lin, S.-H., Chu, P., Hoenderop, J.G.J., and Bindels, R.J.M. (2010). Testosterone increases urinary calcium excretion and inhibits expression of renal calcium transport proteins. *Kidney Int.* 77, 601–608. <https://doi.org/10.1038/ki.2009.522>.
30. Harris, A.N., Lee, H.-W., Verlander, J.W., and Weiner, I.D. (2020). Testosterone modulates renal ammonia metabolism. *Am. J. Physiol. Renal Physiol.* 318, F922–F935. <https://doi.org/10.1152/ajprenal.00560.2019>.
31. Harris, A.N., Castro, R.A., Lee, H.-W., Verlander, J.W., and Weiner, I.D. (2021). Role of the renal androgen receptor in sex differences in ammonia metabolism. *Am. J. Physiol. Renal Physiol.* 321, F629–F644. <https://doi.org/10.1152/ajprenal.00260.2021>.
32. Stringer, K.D., Komers, R., Osman, S.A., Oyama, T.T., Lindsley, J.N., and Anderson, S. (2005). Gender hormones and the progression of experimental polycystic kidney disease. *Kidney Int.* 68, 1729–1739. <https://doi.org/10.1111/j.1523-1755.2005.00589.x>.
33. Metcalfe, P.D., and Meldrum, K.K. (2006). Sex differences and the role of sex steroids in renal injury. *J. Urol.* 176, 15–21. [https://doi.org/10.1016/S0022-5347\(06\)00490-3](https://doi.org/10.1016/S0022-5347(06)00490-3).
34. Ljubojević, M., Balen, D., Breljak, D., Kusan, M., Anzai, N., Bahn, A., Burckhardt, G., and Sabolić, I. (2007). Renal expression of organic anion transporter OAT2 in rats and mice is regulated by sex hormones. *Am. J. Physiol. Renal Physiol.* 292, F361–F372. <https://doi.org/10.1152/ajprenal.00207.2006>.
35. Robert, R., Ghazali, D., Favreau, F., Mauco, G., Hauet, T., and Goujon, J.-M. (2011). Gender difference and sex hormone production in rodent renal ischemia reperfusion injury and repair. *J. Inflamm. (Lond.)* 8, 14. <https://doi.org/10.1186/1476-9255-8-14>.
36. Sabolic, I., Vrhovac, I., Eror, D.B., Gerasimova, M., Rose, M., Breljak, D., Ljubojevic, M., Brzica, H., Sebastiani, A., Thal, S.C., et al. (2012). Expression of Na^+ -D-glucose cotransporter SGLT2 in rodents is kidney-specific and exhibits sex and species differences. *Am. J. Physiol. Cell Physiol.* 302, C1174–C1188. <https://doi.org/10.1152/ajpcell.00450.2011>.

37. Breijak, D., Brzica, H., Sweet, D.H., Anzai, N., and Sabolic, I. (2013). Sex-dependent expression of Oat3 (Slc22a8) and Oat1 (Slc22a6) proteins in murine kidneys. *Am. J. Physiol. Renal Physiol.* 304, F1114–F1126. <https://doi.org/10.1152/ajprel.00201.2012>.

38. Zhang, M.-Z., Sasaki, K., Li, Y., Li, Z., Pan, Y., Jin, G.-N., Wang, Y., Niu, A., Wang, S., Fan, X., et al. (2019). The role of the EGF receptor in sex differences in kidney injury. *J. Am. Soc. Nephrol.* 30, 1659–1673. <https://doi.org/10.1681/ASN.2018121244>.

39. Udy, G.B., Towers, R.P., Snell, R.G., Wilkins, R.J., Park, S.H., Ram, P.A., Waxman, D.J., and Davey, H.W. (1997). Requirement of STAT5b for sexual dimorphism of body growth rates and liver gene expression. *Proc. Natl. Acad. Sci. USA.* 94, 7239–7244. <https://doi.org/10.1073/pnas.94.14.7239>.

40. Waxman, D.J., and O'Connor, C. (2006). Growth hormone regulation of sex-dependent liver gene expression. *Mol. Endocrinol.* 20, 2613–2629. <https://doi.org/10.1210/me.2006-0007>.

41. Meyer, R.D., Laz, E.V., Su, T., and Waxman, D.J. (2009). Male-specific hepatic Bcl6: growth hormone-induced block of transcription elongation in females and binding to target genes inversely coordinated with STAT5. *Mol. Endocrinol.* 23, 1914–1926. <https://doi.org/10.1210/me.2009-0242>.

42. Sugathan, A., and Waxman, D.J. (2013). Genome-wide analysis of chromatin states reveals distinct mechanisms of sex-dependent gene regulation in male and female mouse liver. *Mol. Cell. Biol.* 33, 3594–3610. <https://doi.org/10.1128/MCB.00280-13>.

43. Lau-Corona, D., Suvorov, A., and Waxman, D.J. (2017). Feminization of male mouse liver by persistent growth hormone stimulation: activation of sex-biased transcriptional networks and dynamic changes in chromatin states. *Mol. Cell. Biol.* 37, e00301-17. <https://doi.org/10.1128/MCB.00301-17>.

44. Waxman, D.J., and Kineman, R.D. (2022). Sex matters in liver fat regulation. *Science* 378, 252–253. <https://doi.org/10.1126/science.ade7614>.

45. Takemon, Y., Chick, J.M., Gerdes Gyuricza, I., Skelly, D.A., Devuyst, O., Gygi, S.P., Churchill, G.A., and Korstanje, R. (2021). Proteomic and transcriptomic profiling reveal different aspects of aging in the kidney. *ELife* 10, e62585. <https://doi.org/10.7554/eLife.62585>.

46. Pihlajamaa, P., Sahu, B., Lyly, L., Aittomäki, V., Hautaniemi, S., and Jänne, O.A. (2014). Tissue-specific pioneer factors associate with androgen receptor cistromes and transcription programs. *EMBO J.* 33, 312–326. <https://doi.org/10.1002/embj.201385895>.

47. Miao, Z., Balzer, M.S., Ma, Z., Liu, H., Wu, J., Shrestha, R., Aranyi, T., Kwan, A., Kondo, A., Pontoglio, M., et al. (2021). Single cell regulatory landscape of the mouse kidney highlights cellular differentiation programs and disease targets. *Nat. Commun.* 12, 2277. <https://doi.org/10.1038/s41467-021-22266-1>.

48. Luo, Y., Hitz, B.C., Gabdank, I., Hilton, J.A., Kagda, M.S., Lam, B., Myers, Z., Sud, P., Jou, J., Lin, K., et al. (2020). New developments on the Encyclopedia of DNA Elements (ENCODE) data portal. *Nucleic Acids Res.* 48, D882–D889. <https://doi.org/10.1093/nar/gkz1062>.

49. Kaimal, V., Bardes, E.E., Tabar, S.C., Jegga, A.G., and Aronow, B.J. (2010). ToppCluster: a multiple gene list feature analyzer for comparative enrichment clustering and network-based dissection of biological systems. *Nucleic Acids Res.* 38, W96–W102. <https://doi.org/10.1093/nar/gkq418>.

50. Rada, P., González-Rodríguez, Á., García-Monzón, C., and Valverde, Á.M. (2020). Understanding lipotoxicity in NAFLD pathogenesis: is CD36 a key driver? *Cell Death Dis.* 11, 802. <https://doi.org/10.1038/s41419-020-03003-w>.

51. He, A., Chen, X., Tan, M., Chen, Y., Lu, D., Zhang, X., Dean, J.M., Razani, B., and Lodhi, I.J. (2020). Acetyl-CoA derived from hepatic peroxisomal β-oxidation inhibits autophagy and promotes steatosis via mTORC1 activation. *Mol. Cell* 79, 30–42.e4. <https://doi.org/10.1016/j.molcel.2020.05.007>.

52. Iwai, T., Kume, S., Chin-Kanasaki, M., Kuwagata, S., Araki, H., Takeda, N., Sugaya, T., Uzu, T., Maegawa, H., and Araki, S.-I. (2016). Stearyl-CoA desaturase-1 protects cells against lipotoxicity-mediated apoptosis in proximal tubular cells. *Int. J. Mol. Sci.* 17, 1868. <https://doi.org/10.3390/ijms17111868>.

53. Wang, G., Bonkovsky, H.L., de Lemos, A., and Burczynski, F.J. (2015). Recent insights into the biological functions of liver fatty acid binding protein 1. *J. Lipid Res.* 56, 2238–2247. <https://doi.org/10.1194/jlr.R056705>.

54. Ellis, J.M., Wong, G.W., and Wolfgang, M.J. (2013). Acyl coenzyme A thioesterase 7 regulates neuronal fatty acid metabolism to prevent neurotoxicity. *Mol. Cell. Biol.* 33, 1869–1882. <https://doi.org/10.1128/MCB.01548-12>.

55. Libby, A.E., Jones, B., Lopez-Santiago, I., Rowland, E., and Levi, M. (2021). Nuclear receptors in the kidney during health and disease. *Mol. Aspects Med.* 78, 100935. <https://doi.org/10.1016/j.mam.2020.100935>.

56. Kwekel, J.C., Desai, V.G., Moland, C.L., Vijay, V., and Fuscoe, J.C. (2013). Sex differences in kidney gene expression during the life cycle of F344 rats. *Biol. Sex Differ.* 4, 14. <https://doi.org/10.1186/2042-6410-4-14>.

57. McDowell, I.C., Manandhar, D., Vockley, C.M., Schmid, A.K., Reddy, T.E., and Engelhardt, B.E. (2018). Clustering gene expression time series data using an infinite Gaussian process mixture model. *PLoS Comput. Biol.* 14, e1005896. <https://doi.org/10.1371/journal.pcbi.1005896>.

58. Garcia-Alonso, L., Holland, C.H., Ibrahim, M.M., Turei, D., and Saez-Rodriguez, J. (2019). Benchmark and integration of resources for the estimation of human transcription factor activities. *Genome Res.* 29, 1363–1375. <https://doi.org/10.1101/gr.240663.118>.

59. Holland, C.H., Szalai, B., and Saez-Rodriguez, J. (2020). Transfer of regulatory knowledge from human to mouse for functional genomics analysis. *Biochim. Biophys. Acta Gene Regul. Mech.* 1863, 194431. <https://doi.org/10.1016/j.bbagr.2019.194431>.

60. Keenan, A.B., Torre, D., Lachmann, A., Leong, A.K., Wojciechowicz, M.L., Utti, V., Jagodnik, K.M., Kropiwnicki, E., Wang, Z., and Ma'ayan, A. (2019). ChEA3: transcription factor enrichment analysis by orthogonal omics integration. *Nucleic Acids Res.* 47, W212–W224. <https://doi.org/10.1093/nar/gkz446>.

61. Marable, S.S., Chung, E., and Park, J.-S. (2020). Hnf4a is required for the development of Cd6-expressing progenitors into proximal tubules in the mouse kidney. *J. Am. Soc. Nephrol.* 31, 2543–2558. <https://doi.org/10.1210/ASN.2020020184>.

62. Johnsen, M., Kubacki, T., Yeroslaviz, A., Späth, M.R., Mörsdorf, J., Göbel, H., Bohl, K., Ignarski, M., Meharg, C., Habermann, B., et al. (2020). The integrated RNA landscape of renal preconditioning against ischemia-reperfusion injury. *J. Am. Soc. Nephrol.* 31, 716–730. <https://doi.org/10.1210/ASN.2019050534>.

63. Kobayashi, A., Valerius, M.T., Mugford, J.W., Carroll, T.J., Self, M., Oliver, G., and McMahon, A.P. (2008). Six2 defines and regulates a multipotent self-renewing nephron progenitor population throughout mammalian kidney development. *Cell Stem Cell* 3, 169–181. <https://doi.org/10.1016/j.stem.2008.05.020>.

64. Castro-Mondragon, J.A., Riudavets-Puig, R., Rauluseviciute, I., Lemma, R.B., Turchi, L., Blanc-Mathieu, R., Lucas, J., Boddie, P., Khan, A., Manosalva Pérez, N., et al. (2022). JASPAR 2022: the 9th release of the open-access database of transcription factor binding profiles. *Nucleic Acids Res.* 50, D165–D173. <https://doi.org/10.1093/nar/gkab1113>.

65. El Zein, L., Ait-Lounis, A., Morlé, L., Thomas, J., Chhin, B., Spassky, N., Reith, W., and Durand, B. (2009). RFX3 governs growth and beating efficiency of motile cilia in mouse and controls the expression of genes involved in human ciliopathies. *J. Cell Sci.* 122, 3180–3189. <https://doi.org/10.1242/jcs.048348>.

66. Hennighausen, L., Robinson, G.W., Wagner, K.-U., and Liu, W. (1997). Prolactin signaling in mammary gland development. *J. Biol. Chem.* 272, 7567–7569. <https://doi.org/10.1074/jbc.272.12.7567>.

67. Herrington, J., Smit, L.S., Schwartz, J., and Carter-Su, C. (2000). The role of STAT proteins in growth hormone signaling. *Oncogene* 19, 2585–2597. <https://doi.org/10.1038/sj.onc.1203526>.

Developmental Cell

Article

68. Graves, J.P., Edin, M.L., Bradbury, J.A., Gruzdev, A., Cheng, J., Lih, F.B., Masinde, T.A., Qu, W., Clayton, N.P., Morrison, J.P., et al. (2013). Characterization of four new mouse cytochrome P450 enzymes of the CYP2J subfamily. *Drug Metab. Dispos.* 41, 763–773. <https://doi.org/10.1124/dmd.112.049429>.

69. Hagenbuch, B., Adler, I.D., and Schmid, T.E. (2000). Molecular cloning and functional characterization of the mouse organic-anion-transporting polypeptide 1 (Oatp1) and mapping of the gene to chromosome X. *Biochem. J.* 345, 115–120.

70. Isern, J., Hagenbuch, B., Stieger, B., Meier, P.J., and Meseguer, A. (2001). Functional analysis and androgen-regulated expression of mouse organic anion transporting polypeptide 1 (Oatp1) in the kidney. *Biochim. Biophys. Acta* 1518, 73–78. [https://doi.org/10.1016/s0167-4781\(01\)00169-5](https://doi.org/10.1016/s0167-4781(01)00169-5).

71. Ochiai, Y., Suzuki, C., Segawa, K., Uchiyama, Y., and Nagata, S. (2022). Inefficient development of syncytiotrophoblasts in the *Atp17a*-deficient mouse placenta. *Proc. Natl. Acad. Sci. USA.* 119, e2200582119. <https://doi.org/10.1073/pnas.2200582119>.

72. Sebastian, T.T., Baldridge, R.D., Xu, P., and Graham, T.R. (2012). Phospholipid flippases: building asymmetric membranes and transport vesicles. *Biochim. Biophys. Acta* 1821, 1068–1077. <https://doi.org/10.1016/j.bbalip.2011.12.007>.

73. Andersen, J.P., Vestergaard, A.L., Mikkelsen, S.A., Mogensen, L.S., Chalat, M., and Molday, R.S. (2016). P4-ATPases as phospholipid flippases-structure, function, and enigmas. *Front. Physiol.* 7, 275. <https://doi.org/10.3389/fphys.2016.00275>.

74. Liang, A., Wang, Y., Woodard, L.E., Wilson, M.H., Sharma, R., Awasthi, Y.C., Du, J., Mitch, W.E., and Cheng, J. (2012). Loss of glutathione S-transferase A4 accelerates obstruction-induced tubule damage and renal fibrosis. *J. Pathol.* 228, 448–458. <https://doi.org/10.1002/path.4067>.

75. Fletcher, J.I., Haber, M., Henderson, M.J., and Norris, M.D. (2010). ABC transporters in cancer: more than just drug efflux pumps. *Nat. Rev. Cancer* 10, 147–156. <https://doi.org/10.1038/nrc2789>.

76. Xiao, W., Wang, X., Wang, T., Chen, B., and Xing, J. (2019). HAO2 inhibits malignancy of clear cell renal cell carcinoma by promoting lipid catabolic process. *J. Cell. Physiol.* 234, 23005–23016. <https://doi.org/10.1002/jcp.28861>.

77. Wu, H., Lai, C.F., Chang-Panesso, M., and Humphreys, B.D. (2020). Proximal tubule translational profiling during kidney fibrosis reveals proinflammatory and long noncoding RNA expression patterns with sexual dimorphism. *J. Am. Soc. Nephrol.* 31, 23–38. <https://doi.org/10.1681/asn.2019040337>.

78. Chowen, J.A., Frago, L.M., and Argente, J. (2004). The regulation of GH secretion by sex steroids. *Eur. J. Endocrinol.* 151, U95–U100. <https://doi.org/10.1530/eje.0.151u095>.

79. Meinhardt, U.J., and Ho, K.Y. (2006). Modulation of growth hormone action by sex steroids. *Clin. Endocrinol. (Oxf.)* 65, 413–422. <https://doi.org/10.1111/j.1365-2265.2006.02676.x>.

80. Norheim, F., Hasin-Brumshtain, Y., Vergnes, L., Chella Krishnan, K., Pan, C., Seldin, M.M., Hui, S.T., Mehrabian, M., Zhou, Z., Gupta, S., et al. (2019). Gene-by-sex interactions in mitochondrial functions and cardio-metabolic traits. *Cell Metab.* 29, 932–949.e4. <https://doi.org/10.1016/j.cmet.2018.12.013>.

81. AlOgayil, N., Bauermeister, K., Galvez, J.H., Venkatesh, V.S., Zhuang, Q.K.-W., Chang, M.L., Davey, R.A., Zajac, J.D., Ida, K., Kamiya, A., et al. (2021). Distinct roles of androgen receptor, estrogen receptor alpha, and BCL6 in the establishment of sex-biased DNA methylation in mouse liver. *Sci. Rep.* 11, 13766. <https://doi.org/10.1038/s41598-021-93216-6>.

82. Postic, C., Shiota, M., Niswender, K.D., Jetton, T.L., Chen, Y., Moates, J.M., Shelton, K.D., Lindner, J., Cherrington, A.D., and Magnuson, M.A. (1999). Dual roles for glucokinase in glucose homeostasis as determined by liver and pancreatic beta cell-specific gene knock-outs using Cre recombinase. *J. Biol. Chem.* 274, 305–315. <https://doi.org/10.1074/jbc.274.1.305>.

83. Lopes-Ramos, C.M., Chen, C.-Y., Kuijjer, M.L., Paulson, J.N., Sonawane, A.R., Fagny, M., Platig, J., Glass, K., Quackenbush, J., and DeMeo, D.L. (2020). Sex differences in gene expression and regulatory networks across 29 human tissues. *Cell Rep.* 31, 107795. <https://doi.org/10.1016/j.celrep.2020.107795>.

84. Oliva, M., Muñoz-Aguirre, M., Kim-Hellmuth, S., Wucher, V., Gewirtz, A.D.H., Cotter, D.J., Parsana, P., Kasela, S., Balliu, B., Viñuela, A., et al. (2020). The impact of sex on gene expression across human tissues. *Science* 369, eaba3066. <https://doi.org/10.1126/science.aba3066>.

85. Huang, L., Liao, J., He, J., Pan, S., Zhang, H., Yang, X., Cheng, J., Chen, Y., and Mo, Z. (2020). Single-cell profiling reveals sex diversity in human renal proximal tubules. *Gene* 752, 144790. <https://doi.org/10.1016/j.gene.2020.144790>.

86. Muto, Y., Wilson, P.C., Ledru, N., Wu, H., Dimke, H., Waikar, S.S., and Humphreys, B.D. (2021). Single cell transcriptional and chromatin accessibility profiling redefine cellular heterogeneity in the adult human kidney. *Nat. Commun.* 12, 2190. <https://doi.org/10.1038/s41467-021-22368-w>.

87. Thongnak, L., Pongchaidecha, A., and Lungkaphin, A. (2020). Renal lipid metabolism and lipotoxicity in diabetes. *Am. J. Med. Sci.* 359, 84–99. <https://doi.org/10.1016/j.amjms.2019.11.004>.

88. Wanders, R.J.A., Waterham, H.R., and Ferdinandusse, S. (2015). Metabolic interplay between peroxisomes and other subcellular organelles including mitochondria and the endoplasmic reticulum. *Front. Cell Dev. Biol.* 3, 83. <https://doi.org/10.3389/fcell.2015.00083>.

89. Sultanova, R.F., Schibalski, R., Yankelevich, I.A., Stadler, K., and Ilatovskaya, D.V. (2020). Sex differences in renal mitochondrial function: a hormone-Gous opportunity for research. *Am. J. Physiol. Renal Physiol.* 319, F1117–F1124. <https://doi.org/10.1152/ajrenal.00320.2020>.

90. Scerbo, D., Son, N.-H., Sirwi, A., Zeng, L., Sas, K.M., Cifarelli, V., Schoiswohl, G., Huggins, L.-A., Gumaste, N., Hu, Y., et al. (2017). Kidney triglyceride accumulation in the fasted mouse is dependent upon serum free fatty acids. *J. Lipid Res.* 58, 1132–1142. <https://doi.org/10.1194/jlr.M074427>.

91. Irazabal, M.V., and Torres, V.E. (2020). Reactive oxygen species and redox signaling in chronic kidney disease. *Cells* 9, 1342. <https://doi.org/10.3390/cells9061342>.

92. Ma, Q. (2013). Role of nrf2 in oxidative stress and toxicity. *Annu. Rev. Pharmacol. Toxicol.* 53, 401–426. <https://doi.org/10.1146/annurev-pharmtox-011112-140320>.

93. Saha, S., Buttari, B., Panieri, E., Profumo, E., and Sas, L. (2020). An overview of Nrf2 signaling pathway and its role in inflammation. *Molecules* 25, 5474. <https://doi.org/10.3390/molecules25225474>.

94. Ide, S., Ide, K., Abe, K., Kobayashi, Y., Kitai, H., McKey, J., Strausser, S.A., O'Brien, L.L., Tata, A., Tata, P.R., and Souma, T. (2022). Sex differences in resilience to ferroptosis underlie sexual dimorphism in kidney injury and repair. *Cell Rep.* 41, 111610. <https://doi.org/10.1016/j.celrep.2022.111610>.

95. Liu, Z.-Q., Lee, J.N., Son, M., Lim, J.-Y., Dutta, R.K., Maharjan, Y., Kwak, S., Oh, G.T., Byun, K., Choe, S.-K., and Park, R. (2018). Ciliogenesis is reciprocally regulated by PPARα and NR1H4/FXR through controlling autophagy in vitro and in vivo. *Autophagy* 14, 1011–1027. <https://doi.org/10.1080/15548627.2018.1448326>.

96. Picard, M., and Shirihai, O.S. (2022). Mitochondrial signal transduction. *Cell Metab.* 34, 1620–1653. <https://doi.org/10.1016/j.cmet.2022.10.008>.

97. Harper, J.M., Leathers, C.W., and Austad, S.N. (2006). Does caloric restriction extend life in wild mice? *Aging Cell* 5, 441–449. <https://doi.org/10.1111/j.1474-9726.2006.00236.x>.

98. Cangemi, R., Friedmann, A.J., Holloszy, J.O., and Fontana, L. (2010). Long-term effects of calorie restriction on serum sex-hormone concentrations in men. *Aging Cell* 9, 236–242. <https://doi.org/10.1111/j.1474-9726.2010.00553.x>.

99. Zhang, Y., Laz, E.V., and Waxman, D.J. (2012). Dynamic, sex-differential STAT5 and BCL6 binding to sex-biased, growth hormone-regulated

genes in adult mouse liver. *Mol. Cell. Biol.* 32, 880–896. <https://doi.org/10.1128/MCB.06312-11>.

100. Lau-Corona, D., Ma, H., Vergato, C., Sarmiento-Cabral, A., del Rio-Moreno, M., Kineman, R.D., and Waxman, D.J. (2022). Constitutively active STAT5b feminizes mouse liver gene expression. *Endocrinology* 163, bqac046. <https://doi.org/10.1210/endocr/bqac046>.

101. Sundseth, S.S., and Waxman, D.J. (1992). Sex-dependent expression and clofibrate inducibility of cytochrome P450 4A fatty acid omega-hydroxylases. Male specificity of liver and kidney CYP4A2 mRNA and tissue-specific regulation by growth hormone and testosterone. *J. Biol. Chem.* 267, 3915–3921.

102. Buhr, E.D., Yoo, S.H., and Takahashi, J.S. (2010). Temperature as a universal resetting cue for mammalian circadian oscillators. *Science* 330, 379–385. <https://doi.org/10.1126/science.1195262>.

103. Mantzoros, C.S., Ozata, M., Negrao, A.B., Suchard, M.A., Zioutopoulou, M., Caglayan, S., Elashoff, R.M., Cogswell, R.J., Negro, P., Liberty, V., et al. (2001). Synchronicity of frequently sampled thyrotropin (TSH) and leptin concentrations in healthy adults and leptin-deficient subjects: evidence for possible partial TSH regulation by leptin in humans. *J. Clin. Endocrinol. Metab.* 86, 3284–3291. <https://doi.org/10.1210/jcem.86.7.7644>.

104. Thomson, S.C., and Blantz, R.C. (2012). Biophysics of glomerular filtration. *Compr. Physiol.* 2, 1671–1699. <https://doi.org/10.1002/cphy.c000089>.

105. Gąsiorowski, L., Andrikou, C., Janssen, R., Bump, P., Budd, G.E., Lowe, C.J., and Hejnol, A. (2021). Molecular evidence for a single origin of ultrafiltration-based excretory organs. *Curr. Biol.* 31, 3629–3638.e2. <https://doi.org/10.1016/j.cub.2021.05.057>.

106. Marsh, D.J., Postnov, D.D., Sosnovtseva, O.V., and Holstein-Rathlou, N.-H. (2019). The nephron-arterial network and its interactions. *Am. J. Physiol. Renal Physiol.* 316, F769–F784. <https://doi.org/10.1152/ajrenal.00484.2018>.

107. Wilson, P.C., Muto, Y., Wu, H., Karihaloo, A., Waikar, S.S., and Humphreys, B.D. (2022). Multimodal single cell sequencing implicates chromatin accessibility and genetic background in diabetic kidney disease progression. *Nat. Commun.* 13, 5253. <https://doi.org/10.1038/s41467-022-32972-z>.

108. McEvoy, C.M., Murphy, J.M., Zhang, L., Clotet-Freixas, S., Mathews, J.A., An, J., Karimzadeh, M., Pouyabahar, D., Su, S., Zaslaver, O., et al. (2022). Single-cell profiling of healthy human kidney reveals features of sex-based transcriptional programs and tissue-specific immunity. *Nat. Commun.* 13, 7634. <https://doi.org/10.1038/s41467-022-35297-z>.

109. Grand, K., Stoltz, M., Rizzo, L., Röck, R., Kaminski, M.M., Salinas, G., Getwan, M., Naert, T., Pichler, R., and Lienkamp, S.S. (2023). HNF1B alters an evolutionarily conserved nephrogenic program of target genes. *J. Am. Soc. Nephrol.* 34, 412–432. <https://doi.org/10.1681/ASN.2022010076>.

110. Corkins, M.E., Achieng, M., DeLay, B.D., Kmetta-Stankic, V., Cain, M.P., Walker, B.L., Chen, J., Lindström, N.O., and Miller, R.K. (2023). A comparative study of cellular diversity between the *Xenopus* pronephric and mouse metanephric nephron. *Kidney Int.* 103, 77–86. <https://doi.org/10.1016/j.kint.2022.07.027>.

111. Bankhead, P., Loughrey, M.B., Fernández, J.A., Dombrowski, Y., McArt, D.G., Dunne, P.D., McQuaid, S., Gray, R.T., Murray, L.J., Coleman, H.G., et al. (2017). QuPath: open source software for digital pathology image analysis. *Sci. Rep.* 7, 16878. <https://doi.org/10.1038/s41598-017-17204-5>.

112. Chen, S., Zhou, Y., Chen, Y., and Gu, J. (2018). fastp: an ultra-fast all-in-one FASTQ preprocessor. *Bioinformatics* 34, i884–i890. <https://doi.org/10.1093/bioinformatics/bty560>.

113. Dobin, A., Davis, C.A., Schlesinger, F., Drenkow, J., Zaleski, C., Jha, S., Batut, P., Chaisson, M., and Gingeras, T.R. (2013). STAR: ultrafast universal RNA-seq aligner. *Bioinformatics* 29, 15–21. <https://doi.org/10.1093/bioinformatics/bts635>.

114. Liao, Y., Smyth, G.K., and Shi, W. (2014). featureCounts: an efficient general purpose program for assigning sequence reads to genomic features. *Bioinformatics* 30, 923–930. <https://doi.org/10.1093/bioinformatics/btt656>.

115. Love, M.I., Huber, W., and Anders, S. (2014). Moderated estimation of fold change and dispersion for RNA-seq data with DESeq2. *Genome Biol.* 15, 550. <https://doi.org/10.1186/s13059-014-0550-8>.

116. Pimentel, H., Bray, N.L., Puente, S., Melsted, P., and Pachter, L. (2017). Differential analysis of RNA-seq incorporating quantification uncertainty. *Nat. Methods* 14, 687–690. <https://doi.org/10.1038/nmeth.4324>.

117. Lin, K.T., and Krainer, A.R. (2019). PSI-Sigma: a comprehensive splicing-detection method for short-read and long-read RNA-seq analysis. *Bioinformatics* 35, 5048–5054. <https://doi.org/10.1093/bioinformatics/btz438>.

118. Love, M.I., Soneson, C., and Patro, R. (2018). Swimming downstream: statistical analysis of differential transcript usage following Salmon quantification. *F1000Res* 7, 952. <https://doi.org/10.12688/f1000research.15398.3>.

119. Hao, Y., Hao, S., Andersen-Nissen, E., Mauck, W.M., III, Zheng, S., Butler, A., Lee, M.J., Wilk, A.J., Darby, C., Zager, M., et al. (2021). Integrated analysis of multimodal single-cell data. *Cell* 184, 3573–3587.e29. <https://doi.org/10.1016/j.cell.2021.04.048>.

120. Stuart, T., Srivastava, A., Madad, S., Lareau, C.A., and Satija, R. (2021). Single-cell chromatin state analysis with Signac. *Nat. Methods* 18, 1333–1341. <https://doi.org/10.1038/s41592-021-01282-5>.

121. Young, M.D., and Behjati, S. (2020). SoupX removes ambient RNA contamination from droplet-based single-cell RNA sequencing data. *Gigascience* 9, giaa151. <https://doi.org/10.1093/gigascience/giaa151>.

122. McGinnis, C.S., Murrow, L.M., and Gartner, Z.J. (2019). DoubletFinder: doublet detection in single-cell RNA sequencing data using artificial nearest neighbors. *Cell Syst.* 8, 329–337.e4. <https://doi.org/10.1016/j.cels.2019.03.003>.

123. Granza, J.M., Corces, M.R., Pierce, S.E., Bagdatti, S.T., Choudhry, H., Chang, H.Y., and Greenleaf, W.J. (2021). ArchR is a scalable software package for integrative single-cell chromatin accessibility analysis. *Nat. Genet.* 53, 403–411. <https://doi.org/10.1038/s41588-021-00790-6>.

124. Zhang, Y., Liu, T., Meyer, C.A., Eeckhoute, J., Johnson, D.S., Bernstein, B.E., Nusbaum, C., Myers, R.M., Brown, M., Li, W., and Liu, X.S. (2008). Model-based analysis of ChIP-seq (MACS). *Genome Biol.* 9, R137. <https://doi.org/10.1186/gb-2008-9-9-r137>.

125. Yu, D., Huber, W., and Vitek, O. (2013). Shrinkage estimation of dispersion in Negative Binomial models for RNA-seq experiments with small sample size. *Bioinformatics* 29, 1275–1282. <https://doi.org/10.1093/bioinformatics/btt143>.

126. Bailey, T.L., Johnson, J., Grant, C.E., and Noble, W.S. (2015). The MEME Suite. *Nucleic Acids Res.* 43, W39–W49. <https://doi.org/10.1093/nar/gkv416>.

127. Langmead, B., and Salzberg, S.L. (2012). Fast gapped-read alignment with Bowtie 2. *Nat. Methods* 9, 357–359. <https://doi.org/10.1038/nmeth.1923>.

128. Danecek, P., Bonfield, J.K., Liddle, J., Marshall, J., Ohan, V., Pollard, M.O., Whitwham, A., Keane, T., McCarthy, S.A., Davies, R.M., and Li, H. (2021). Twelve years of SAMtools and BCFtools. *Gigascience* 10, giab008. <https://doi.org/10.1093/gigascience/giab008>.

129. Kent, W.J., Zweig, A.S., Barber, G., Hinrichs, A.S., and Karolchik, D. (2010). BigWig and BigBed: enabling browsing of large distributed datasets. *Bioinformatics* 26, 2204–2207. <https://doi.org/10.1093/bioinformatics/btq351>.

130. Wilson, P.C., Wu, H., Krita, Y., Uchimura, K., Ledru, N., Rennke, H.G., Welling, P.A., Waikar, S.S., and Humphreys, B.D. (2019). The single-cell transcriptomic landscape of early human diabetic nephropathy. *Proc. Natl. Acad. Sci. USA* 116, 19619–19625. <https://doi.org/10.1073/pnas.1908706116>.

131. Robinson, M.D., and Oshlack, A. (2010). A scaling normalization method for differential expression analysis of RNA-seq data. *Genome Biol.* 11, R25. <https://doi.org/10.1186/gb-2010-11-3-r25>.

132. Klopfenstein, D.V., Zhang, L., Pedersen, B.S., Ramírez, F., Warwick Vesztrocy, A., Naldi, A., Mungall, C.J., Yunes, J.M., Botvinnik, O., Weigel, M., et al. (2018). GOATOOLS: a Python library for Gene Ontology analyses. *Sci. Rep.* 8, 10872. <https://doi.org/10.1038/s41598-018-28948-z>.
133. Gerhardt, L.M.S., Liu, J., Koppitch, K., Cippà, P.E., and McMahon, A.P. (2021). Single-nuclear transcriptomics reveals diversity of proximal tubule cell states in a dynamic response to acute kidney injury. *Proc. Natl. Acad. Sci. USA.* 118, e2026684118. <https://doi.org/10.1073/pnas.2026684118>.
134. Janssens, J., Aibar, S., Taskiran, I.I., Ismail, J.N., Gomez, A.E., Aughey, G., Spanier, K.I., De Rop, F.V., González-Blas, C.B., Dionne, M., et al. (2022). Decoding gene regulation in the fly brain. *Nature* 601, 630–636. <https://doi.org/10.1038/s41586-021-04262-z>.
135. Kulakovskiy, I.V., Vorontsov, I.E., Yevshin, I.S., Sharipov, R.N., Fedorova, A.D., Rumynskiy, E.I., Medvedeva, Y.A., Magana-Mora, A., Bajic, V.B., Papatsenko, D.A., et al. (2018). HOCOMOCO: towards a complete collection of transcription factor binding models for human and mouse via large-scale ChIP-Seq analysis. *Nucleic Acids Res.* 46, D252–D259. <https://doi.org/10.1093/nar/gkx1106>.

STAR★METHODS

KEY RESOURCES TABLE

REAGENT or RESOURCE	SOURCE	IDENTIFIER
Antibodies		
LTL lectin-FITC conjugate	Vector Laboratories	Cat# FL-1321; RRID: AB_2336559
Goat polyclonal anti-CA4(Car4)	R&D	Cat# AF2414; RRID: AB_2070332
Rabbit polyclonal anti-SGLT2 (Slc5a2)	Abcam	Cat# ab85626; RRID: AB_10674183
Rabbit monoclonal anti- Aquaporin 1	Abcam	Cat# ab168387; RRID: AB_2810992
Chemicals, peptides, and recombinant proteins		
Testosterone	Sigma-Aldrich	T1500; CAS: 58-22-0
Probes for RNA in situ		
RNAscope® Probe- Mm-Prlr-C2	Advanced Cell Diagnostics	430791-C2
RNAscope® Probe- Mm-Gsta4-C1	Advanced Cell Diagnostics	1132411-C1
RNAscope® Probe- Mm-Slco1a1	Advanced Cell Diagnostics	831051
RNAscope® Probe- Mm-Hao2-C1	Advanced Cell Diagnostics	1201591-C1
RNAscope® Probe- Mm-Slco1a1	Advanced Cell Diagnostics	831051
RNAscope® Probe- Mm-Atp11a-C3	Advanced Cell Diagnostics	489841-C3
RNAscope® Probe- Mm-Abcc3-C3	Advanced Cell Diagnostics	1201571-C3
RNAscope® Probe- Mm-Cyp2j13-C3	Advanced Cell Diagnostics	1201581-C3
RNAscope® Probe- Mm-Cyp7b1-C2	Advanced Cell Diagnostics	471001-C2
Deposited data		
Raw and analyzed bulk RNA-seq data	This paper	GEO: GSE225622
Raw and processed single-nuclear multiomic data	This paper	GEO: GSE225566
Experimental models: Organisms/strains		
Mouse: C57BL/6J	The Jackson Laboratory	JAX: 000664
Mouse: B6(Cg)-Esr1tm4.1Ksk/J	The Jackson Laboratory	JAX: 032173
Mouse: B6.129S1-Artm2.1Reb/J	The Jackson Laboratory	JAX: 018450
Mouse: C57BL/6	The Charles River Laboratories	C57BL/6NCrl inbred
Software and algorithms		
DPGP	McDowell et al. ⁵⁷	https://github.com/PrincetonUniversity/DP_GP_cluster
DoRothEA	Garcia-Alonso et al. ⁵⁸ Holland et al. ⁵⁹	https://bioconductor.org/packages/release/data/experiment/html/dorothea.html
ChEA3	Keenan et al. ⁶⁰	https://maayanlab.cloud/chea3/
QuPath	Bankhead et al. ¹¹¹	https://github.com/qupath/qupath
fastp	Chen et al. ¹¹²	https://github.com/OpenGene/fastp
STAR	Dobin et al. ¹¹³	https://code.google.com/archive/p/ma-star/
FeatureCounts	Liao et al. ¹¹⁴	https://subread.sourceforge.net
DESeq2	Love et al. ¹¹⁵	http://www.bioconductor.org/packages/release/bioc/html/DESeq2.html
Kallisto-Sleuth	Pimentel et al. ¹¹⁶	https://github.com/pachterlab/kallisto
PSI-Sigma	Lin et al. ¹¹⁷	https://github.com/wososa/PSI-Sigma
DRIMSeq	Love et al. ¹¹⁸	https://github.com/gosianow/DRIMSeq
Seurat	Hao et al. ¹¹⁹	https://satijalab.org/seurat/
Signac	Stuart et al. ¹²⁰	https://stuartlab.org/signac/
SoupX	Young and Behjati ¹²¹	https://github.com/constantAmateur/SoupX
DoubletFinder	McGinnis et al. ¹²²	https://github.com/chris-mcginnis-ucsf/DoubletFinder

(Continued on next page)

Continued

REAGENT or RESOURCE	SOURCE	IDENTIFIER
ArchR	Granja et al. ¹²³	https://github.com/GreenleafLab/ArchR
MACS2	Zhang et al. ¹²⁴	https://pypi.org/project/MACS2/
sSeq	Yu et al. ¹²⁵	https://bioconductor.org/packages/release/bioc/html/sSeq.html
MEME Suite	Bailey et al. ¹²⁶	https://meme-suite.org/meme/
bowtie2	Langmead and Salzberg ¹²⁷	https://github.com/BenLangmead/bowtie2
SAMtools	Danecek et al. ¹²⁸	https://github.com/samtools/samtools
bedGraphToBigWig	Kent et al. ¹²⁹	https://www.encodeproject.org/software/bedgraphtobigwig/
Customized Code	This paper	https://github.com/LingyunXiong/Kidney_SexDiff

RESOURCE AVAILABILITY

Lead Contact

Further information and requests for resources and reagents should be directed to and will be fulfilled by the lead contact, Andrew P. McMahon (amcmahon@med.usc.edu).

Materials Availability

This study did not generate new unique reagents.

Data and Code Availability

- RNA-seq data have been deposited at Gene Expression Omnibus and are publicly available as of the date of publication. Accession numbers are listed in the [key resources table](#).
- All original code has been deposited on GitHub (Zenodo archive: <https://doi.org/10.5281/zenodo.8208547>).
- Any additional information required to reanalyze the data reported in this paper is available from the [lead contact](#) upon request.

EXPERIMENTAL MODEL AND STUDY PARTICIPANT DETAILS

Institutional Animal Care and Use Committees (IACUC) at the University of Southern California reviewed and approved all animal work as performed in this study. All work adhered to institutional guidelines. Mice from the following strains were from the Jackson Laboratory: C57BL/6J (stock no. 000664), B6(Cg)-Esr1tm4.1Ksk/J (stock no. 032173), B6.129S1-Artm2.1Reb/J, (stock no. 018450), Six2TGC/+ mice were generated as described previously.⁶³ Castrated males and ovariectomized females and control C57BL/6NCrl mice were from Charles River Laboratories.

Husbandry conditions of experimental animals

Animals were either purchased from suppliers as indicated or bred in-house, and genotyping and mating was performed as indicated for specific experiments prior to weaning at 3 weeks *post partum*. The animals were inspected daily for health issues by the staff of the Keck School of Medicine's Department of Animal Resources (DAR) and any health issues addressed in line with recommendations from the veterinary staff. Cages were changed on a routine basis determined by the DAR. All husbandry was carried out under the guidance of the Keck School of Medicine Department of Animal Resources with approval from institutional animal care and use committee.

Housing conditions of experimental animals

Animals were housed individually or in groups depending on age and sex in microisolator cages with filter air supply and feed and water supplied *ad libitum*. All animals housing was carried out under the guidance of the Keck School of Medicine Department of Animal Resources with approval from institutional animal care and use committee.

METHOD DETAILS

RNA-seq

Whole kidney total RNA was extracted using Qiagen's RNeasy Mini Kit and submitted to the Genome Access Technology Center at the McDonnell Genome Institute. Samples were prepared according to Clontech SMARTer library kit manufacturer's protocol, indexed, pooled, and sequenced on Illumina HiSeq2500 platform for 50-bp single-end, and Illumina NovaSeq S4 for 150-bp pair-ended sequencing.

Single-nucleus multimodal experiment

C57BL/6J adult mice (age: 9-12 weeks old; sex: males weighing 21.5-23.2 grams and females weighing 18.4-19.4 grams) were euthanized with CO₂ chamber and perfused with ice cold HPBS (Hyclone). The kidney capsules were removed, and kidneys cut into 6 smaller pieces and flash frozen in liquid nitrogen for further processing. On the day of library preparation, nuclei were isolated as previously described.¹³⁰ Briefly, flash frozen kidney pieces were thawed on ice and minced into small pieces (<1mm) with a sterile razor blade and then dounced in Nuclei EZ Lysis Buffer (Sigma) with Protease Inhibitor. The tissue was dounced 15X loose, filtered with a 200uM filter, and then 5X tight, incubated for 5 mins on ice, filtered through 40uM filter and spun down at 500G x 5min at 4°C in a swinging bucket centrifuge. Supernatant was removed and nuclei pellet resuspended in Nuclei EZ lysis buffer, incubated an additional 5 mins on ice and spin down again. The final pellet was resuspended in Diluted Nuclei Buffer provided in the 10X Chromium Kit and passed through a pre-wetted 5uM filter. All buffers had 1U/ul Protector Rnase inhibitor and 1mM DTT added to preserve RNA integrity. Nuclei were then counted on a Countess III machine and the targeted number (~9,000 nuclei/sample) was loaded into a GEM J Chip as per manufacturer's specifications. Multiomic (10x – PN:10002805) reagents and index plates were used to generate the snATACSeq and snRNASeq libraries. Libraries were processed using 10X Genomics Manual CG000338 (7 preAmp, 8 ATAC library construction, 8 cDNA, 16 GTEX Sample Index – PCR cycles) Libraries were checked by BioAnalyzer before sending to Novogene for NovaSeq6000 S4 PE150 sequencing using Illumina platform.

Fluorescence RNA *in situ* hybridization

RNA *In situ* hybridizations were performed following RNAscope Multiplex Fluorescent Reagent Kit v2 user manual (Advanced Cell Diagnostics) as previously described.¹⁹ We used antibodies for immunofluorescent co-staining on the same frozen sections with RNA probes: LTL lectin-FITC conjugate (#FL-1321; Vector Laboratories); Aqp1 (# ab168387, rabbit; Abcam), SGLT2 (Slc5a2) (# ab85626, rabbit; Abcam), Car4 (#AF2414, goat; R&D). Number of subcellular dots from RNAscope experiments were quantified through QuPath.¹¹¹ Briefly, cells were detected by nucleus staining, then only the spots of target gene with positive PT-segment marker expression were counted.

QUANTIFICATION AND STATISTICAL ANALYSIS

Bulk RNA-seq Data Analysis

Bulk RNA-seq data generated in this study and public data (kidney: GSE121330; liver: GSE112947 and GSE174535) were analyzed using a custom workflow, which is available on GitHub and briefly described in the following. First, raw sequence reads were pre-processed using *fastp*¹¹² (version 0.23.2), which was used to trim low quality (quality score <=20) and to filter short reads (<=20bp). Sequence reads passing quality control were aligned to mouse genome build mm39 (GRCm39) using *STAR*¹¹³ (version 2.7.0) and those that mapped to annotated genomic regions (GENCODE release M28) were counted using *FeatureCounts*¹¹⁴ (version 2.0.3). Differential expression analysis was performed using *DESeq2*.¹¹⁵ Genes with low count per million values (CPM<1) were excluded, and differentially expressed genes were identified based on thresholds of adjusted *P*-value (<0.05) and absolute log₂ fold change (>0.5; i.e., greater than 1.41-fold). Overall sample variation was evaluated by principal component analysis implemented in *DESeq2*, and batch effect (if present) was accounted for by specifying batch information as a covariate in the regression model. Average TMM-normalized gene expression¹³¹ was used as input for heatmap visualization, and scaled expression levels across developmental timepoints or treatment conditions were shown.

Isoform analysis

Isoform expression of known Ensembl transcripts were estimated with Kallisto.¹¹⁶ For all the analyses, only transcripts with (a) adjusted *P*-values < 0.05, (b) absolute log₂ fold change > 0.5, and (c) TPM > 1 were kept. Alternative splicing analysis was performed using PSI-Sigma¹¹⁷ with default settings. Differential transcript usage was identified using DRIMSeq.¹¹⁸ A3SS: alternative 3' splice site; A5SS: alternative 5' splice site; IR: intron retention; MES: multi-exon skipping; SES: single exon skipping; TSS: transcription start site.

Functional Inference

Pathway enrichment analysis of sex-biased genes was performed using *ToppCluster* web browser⁴⁹ with default settings. We used GOATOOLS¹³² for gene ontology analysis, where only terms of biological processes were considered, and multiple testing correction was performed with the Benjamini-Hochberg method.

Computational prediction of upstream regulators

Temporal co-regulation of sex-biased genes was studied using *DPGP*,⁵⁷ where difference in average TMM-normalized gene expression between male and female samples over 5 timepoints were clustered based on shared dynamical features. Clusters with the most genes were prioritized for visualization. Scaled expression levels were shown. The *DoRothEA*^{58,59} and *ChEA3* web browser⁶⁰ were used to infer upstream regulators of sex-biased programs in the kidney. The input for *DoRothEA* was TMM-normalized expression of sex-biased genes or known proximal tubule markers; only high-confidence regulons (class A and B) were used to compute normalized enrichment score (NES) of curated TFs. Given the M- or F-biased genes, *ChEA3* ranked TFs by weighing and integrating extensive ChIP-seq and co-expression evidence for putative TF-target relationship. Mean rank was used in this study. The top 15 TFs were

selected to view co-expression networks, whose expression levels in proximal tubule were checked against previous scRNA-seq data¹⁹ (<https://cello.shinyapps.io/kidneycellexplorer/>). Putative target genes of top-ranked TFs predicted by *ChEA3* were examined for relative impact and overlaps.

Single-nuclear multimodal data processing

We used *Seurat*¹¹⁹ (version 4.1.0) and *Signac*¹²⁰ (version 1.5.0) in R (version 4.0) for primary multimodal (RNA and ATAC) data processing, following the guidelines provided by the software developers. Briefly, we loaded both modalities for each sample and merged counts into a single data object for general data quality evaluation. We assessed ambient RNA contamination in each sample using *SoupX*,¹²¹ to find that the global contamination was 2-4%. Doublets were detected using *DoubletFinder*,¹²² and were filtered together with low-quality cells by the following cut-offs: RNA feature (250-7,000), percentage of mitochondrial RNA (<35%), total ATAC count (1,000-100,000), nucleosome signal (<2) and transcription start site (TSS) enrichment score (>1).

RNA-data were log-normalized and scaled based on the top 2,000 variable features and the data were projected to lower dimension using principal component analysis (PCA). After evaluation of elbow and jackstraw plots, the top 30 principal components were used for k-nearest neighbor (kNN)-based clustering, with a resolution of 0.5. Considering known biological differences between male and female kidneys, we pooled samples using reciprocal PCA-based integration method implemented in *Seurat*. ATAC-data were processed using performing widely implemented latent semantic indexing (LSI) method. We performed term frequency-inverse document frequency (TF-IDF) normalization, followed by top feature identification and singular value decomposition. Leveraging information from both data modalities, the joint neighbor graph was constructed for final clustering using the weighted nearest neighbor methods implemented in *Seurat*. Clustering outcomes were visualized in UMAP plots, where depth imbalance was noted between male and female samples. Features enriched for individual clusters were identified by Wilcoxon rank-sum test with a cutoff for minimum \log_2 fold change (>0.25) and minimum percentage of cells with expression (>0.25). For cell type annotation, top features of each cluster were compared against established markers for broad cell types known to be present in the kidney.^{19,133} Normalized gene expression data were visualized in feature, dot, and violin plots; normalized peak counts were visualized in coverage plots with peaks highlighted.

We used *ArchR*¹²³ (version 1.0.1) for additional multimodal data processing. Besides standard filtering criteria as above and iterative LSI dimensionality reduction with default settings, we created pseudo-bulk replicates for each cluster and performed customized peak calling using *MACS2*¹²⁴ with an FDR cutoff of 0.05. Besides standard genomic features, the peak matrix was also annotated with canonical TF motif using the motif set curated by the Jasper 2022 CORE database⁶⁴ (*Mus musculus*) for AR (MA0007.3) and Hnf4a (MA0114.3), as well as publicly available ChIP-seq data for AR and Hnf4a (see below). The peak matrix was then categorized by the distance to the nearest TSS: peaks within 1 kb of TSS were categorized as proximal peaks; peaks within 100kb but not within 1 kb of TSS were categorized as distal peaks.

Single-nucleus multimodal differential analysis

To identify differentially expressed genes between two annotated clusters of interest, we performed proportional fitting-based depth normalization on raw read counts to mitigate depth imbalance, before applying *sSeq*¹²⁵ as described previously,¹⁹ with a cutoff of adjusted P -value < 0.05 and absolute \log_2 fold change > 0.5 (i.e., greater than 1.44-fold). *sSeq* is a shrinkage-based method for estimating dispersion in negative binomial models for RNA-seq data, well suited for small sample sizes. Briefly, we treated annotated clusters as meta-cells, and computed average normalized gene expression and proportion of non-zero expression cells for each gene across meta-cells. We identified differentially expressed genes for each PT segment separately. The number of differentially expressed genes recovered at meta-cells was significantly higher than those detected at single-cell level, and the signals were shown to be more robust and comprehensive.¹⁹

We identified differentially accessible regions (DARs) between two clusters of interest using Wilcoxon test, adjusted for TSS enrichment score and number of unique fragments per cell, with a cutoff of FDR < 0.05 and absolute \log_2 fold change > 0.25. DAR identification was performed for each segment of the PT cell types. Intersections of the pairwise DARs were categorized and visualized with upset function in *UpSetR* package. To identify DARs that are differentially open in the male WT compared to female WT and male KO, we found the intersection of male WT vs female WT DARs and male WT vs male KO DARs, each with positive \log_2 fold-change value for male WT. To identify DARs that are differentially closed in the male WT compared to female WT and male KO, we found the intersection of male WT vs female WT DARs and male WT vs male KO DARs, this time with negative \log_2 fold-change value for the male WT. DARs were examined for nearest genomic features and TF motif/binding enrichment, based on original peak annotations specified above.

Gene accessibility score

The gene accessibility score ψ is a metric that quantifies how open a genomic region is by summing peak access within a gene body and some distance upstream of its transcription start site (TSS), weighted by the distance of the peak to the TSS and the variability in peak accessibility across cell types, as defined by Janssens et al.¹³⁴ In this study, we used normalized accessibility of each peak per cell as the input, including all peaks inside the gene body and up to 5kb upstream of TSS, but excluding peaks residing within the body of nearby genes. The gene accessibility score was computed as the weighted sum of individual peak accessibility, where the total weight for each peak is the product of the distance and the variation weight. The distance weight is assigned to each peak using an exponentially decaying function so that peaks further away from the TSS are given lower priority, as implemented

by the function of calculating gene score in *ArchR*. To prioritize peaks with variable or differential accessibility across cell types, we calculate the Gini coefficient of each peak among all clusters and use the z-normalized Gini coefficient as the exponent for the variation weight. For visualizing accessibility of selected genes in the heatmap (Figure 6D), the gene accessibility score calculated for each gene was scaled by the maximal value across clusters.

$$\psi = \sum_i (w_d * w_v) * x_i,$$

$$w_d = e^{-\frac{\text{distance to TSS}}{5000}} + e^{-1},$$

$$w_v = e^{z_{\text{Gini}}},$$

where x_i was the normalized peak count.

Motif Analysis

Matching of canonical TF motifs was performed using the Find Individual Motif Occurrences (FIMO) function in MEME Suite¹²⁶ (version 5.5.0), where we supplied PWM information for AR (MA0007.3) and Hnf4a (MA0114.3) from the Jasper 2022 CORE database⁶⁴ (*Mus musculus*). We identified annotated TF motifs that are enriched among peak sets of interest using the Simple Enrichment Analysis (SEA) function in MEME Suite¹²⁶ (version 5.5.0), by specifying the motif database to be HOCOMOCO mouse (v11 full).¹³⁵ We used a *p*-value cut-off of 1E-5 for motif matching and enrichment analysis. Either random genomic regions with matching GC-content or shuffled input sequences were used as the background for comparison. Multiple-hypothesis testing correction was performed using the Benjamini-Hochberg method.

ChIP-seq data processing

Public ChIP-seq data for AR and Hnf4a binding sites in adult kidney tissues (GSE47194⁴⁶) were processed through a custom pipeline developed in the lab. First, raw sequence reads were pre-processed using *fastp* (version 0.23.2¹¹²), during which reads were trimmed and reads of low quality (quality score <= 20) and short length (<= 20bp) were filtered. Sequence reads passing quality control were aligned to mouse genome build mm10 (GRCm38) using *bowtie2*¹²⁷ (version 2.3.5) and *SAMtools*¹²⁸ (version 1.10). Peaks mapped to annotated genomic regions (GENCODE release M22) were called for TF-treated bam files against controls using *MACS2*¹²⁴ with an FDR cutoff of 0.05, specifying no lambda or model, and allowing for a shift size of 75 base pairs and extension size of 150 base pairs. If ChIP-seq experiment was repeated (such as AR-ChIP-seq in GSE47194), replicated peaks were defined as TF-binding sites. In the multimodal data, all accessible peaks overlapping with TF-binding sites with a maximum gap of 250 base pairs were annotated as TF-bound. We used *bedGraphToBigWig*¹²⁹ software (version 2.8) to convert the peak files to bigwig files for genome browser visualization.